Received 8 June 2025; revised 10 July 2025; accepted 13 July 2025. Date of publication 18 July 2025;
date of current version 31 July 2025. The review of this article was arranged by Associate Editor H. Vahedi.

Digital Object Identifier 10.1109/OJIES.2025.3590609

A Concept for Improving Battery Energy Storage System Performance in a Redundant DC Microgrid Without SoC-Based Droop

THALES AUGUSTO FAGUNDES [1], LUCAS JONYS RIBEIRO SILVA [1] (Student Member, IEEE), MÁRCIO VON RONDOW CAMPOS [1], MARINA SILVA CAMILLO DE CARVALHO [1], BRUNO MENEGHEL ZILLI [2], GUILHERME HENRIQUE FAVARO FUZATO [3] (Member, IEEE), AND RICARDO QUADROS MACHADO [1] (Senior Member, IEEE)

[1]Sao Carlos School of Engineering, University of Sao Paulo, Sao Carlos 13566-590, Brazil
[2]Federal University of Technology—Paraná, Guarapuava 85053-525, Brazil
[3]School of Electrical and Computer Engineering, University of Campinas, Campinas 13083-852, Brazil

CORRESPONDING AUTHOR: THALES AUGUSTO FAGUNDES (e-mail: thales.fagundes@usp.br).

This work was supported in part by the Coordination for the Improvement of Higher Education Personnel (CAPES) under Grant PDSE-88881.187771/2018-01, Grant 88881.030370/2013-0, Grant 88887.482911/2020-00, and Grant 88887.182131/2025-00, in part by the National Council for Scientific and Technological Development (CNPq) under Grant 309624/2018-5 and Grant 312664/2021-4, and in part by the Sao Paulo Research Foundation (FAPESP), Brasil. Process under Grant #2013/20721-4, Grant #2020/05865-3, Grant #2022/00628-9, and Grant #2024/00607-7.

ABSTRACT The redundancy strategy enhances the reliability of applications, such as medical centers, shipboard microgrids (MGs), and aircraft systems. This article proposes a redundancy-based dc MG integrating two modules: a cascaded bidirectional Cuk converter (CBC) and a cascaded bidirectional boost converter (CBB), each supported by battery energy storage systems (BESS), improving the reliability in case of module failure. In addition, a boost converter integrates the fuel cell (FC) through the CBC dc-link, employing a droop controller to regulate power production. In this context, the energy management system (EMS) balances the state of charge (SoC) among BESS units using a fuzzy-based method, avoiding SoC-based droop control and addressing nonlinearities in SoC equalization. The EMS also mitigates rapid transients due to load maneuvers on the dc link by using BESS units, and reduces stress on the FC membranes. Considering the CBB, the reliability of the BESS units is improved through battery-to-battery (B2B) equalization, enabled by the fuzzy-based method able to provide current references, thereby increasing power sharing accuracy. Therefore, the proposed solution performs improvement in the BESS equalization process, with redundancy ensuring stable dc-link voltage even during faults. Finally, infinity norm and Lyapunov's indirect method confirm the MG stability, while lab-scale prototype demonstrates experimentally effectiveness.

INDEX TERMS Battery energy storage system (BESS), cascaded bidirectional boost (CBB), cascaded bidirectional Cuk (CBC), fuzzy-based method, state-of-charge (SoC) equalization.

NOMENCLATURE

Abbreviations

BESS	Battery energy storage system.
CBC	Cascaded bidirectional Cuk.
CBB	Cascaded bidirectional boost.
EMS	Energy management system.
MG	Microgrid.
FC	Fuel cell.
SoC	State of charge.
PV	Photovoltaic.
PI	Proportional-integral.
HIL	Hardware-in-the-loop.
PWM	Pulsewidth modulation.

Variables and Constants

v_{bat}	Battery terminal voltage [V].
OCV	Open-circuit voltage of the battery [V].
i_{bat}	Battery current [A].
r_{bat}	Battery internal resistance [Ω].
r_{bat1}	Parameter modeling relaxation resistance [Ω].
C_{bat1}	Parameter modeling relaxation capacitance [F].
$\mathrm{SoC}(t)$	SoC at time t [%].
$\mathrm{SoC}(t_0)$	Initial SoC [%].
C_{bat}	Nominal battery capacity [Ah].
C_1	Capacitance in Cuk1 [F].
C_2	Capacitance in Cuk2 [F].
C_3	DC-link capacitance in CBB [F].
C_o	DC-link capacitance [F].
v_{bat1}	Terminal voltage of BESS1 [V].
v_{bat2}	Terminal voltage of BESS2 [V].
i_{bat1}	Current of BESS1 [A].
i_{bat2}	Current of BESS2 [A].
i_{L1}	Inductance current in Cuk1 [A].
i_{L2}	Inductance current in Cuk1 [A].
i_{L3}	Inductance current in Cuk2 [A].
i_{L4}	Inductance current in Cuk2 [A].
i_{L5}	Inductance current in CBB [A].
i_{L6}	Inductance current in CBB [A].
L_1	Inductance in Cuk1 [H].
L_2	Inductance in Cuk1 [H].
L_3	Inductance in Cuk2 [H].
L_4	Inductance in Cuk2 [H].
L_5	Inductance in CBB [H].
L_6	Inductance in CBB [H].
S_1	Controlled switch Cuk1.
S_2	Controlled switch Cuk2.
S_3	Controlled switch in CBB.
S_4	Controlled switch in CBB.
$\bar{S}_1$	Complementary switch for S_1.
$\bar{S}_2$	Complementary switch for S_2.
$\bar{S}_3$	Complementary switch for S_3.
$\bar{S}_4$	Complementary switch for S_4.
v_o	Main dc-link voltage [V].
R_o	DC load resistance [Ω].
i_o	DC load current [A].
P_{load}	DC load power [W].
v_{C3}	Voltage on CBB dc-link [V].
r_{Li}	Inductance parasitic resistances [Ω].
r_{Si}	Semiconductor parasitic resistances [Ω].
$r_{\bar{S}i}$	Complementary semiconductor parasitic resistances [Ω].
r_{C1}	Capacitance parasitic resistance [Ω].
r_{C2}	Capacitance parasitic resistance [Ω].
r_{C3}	Capacitance parasitic resistance [Ω].
r_{Co}	DC-link capacitance parasitic resistance [Ω].
r_{Sfc}	Semiconductor parasitic resistance [Ω].
Δv_o	Voltage deviation from v_{o_min} [V].
v_{o_min}	Minimum allowed dc-link voltage [V].
$\Delta v_{o\_\mathrm{max}}$	Maximum voltage deviation in droop control [V].
Δv_{C3}	Voltage deviation on CBB dc-link [V].
v_{C3_min}	Minimum voltage of CBB dc-link [V].
SoC_1	SoC of BESS1 [%].
SoC_2	SoC of BESS2 [%].
i_{L1_fuzzy}	Fuzzy logic output for i_{L1} [p.u.].
i_{L3_fuzzy}	Fuzzy logic output for i_{L3} [p.u.].
i_{L5_fuzzy}	Fuzzy logic output for i_{L5} [p.u.].
i_{L6_fuzzy}	Fuzzy logic output for i_{L6} [p.u.].
i_{L1_ref}	Current reference for i_{L1} [A].
i_{L3_ref}	Current reference for i_{L3} [A].
i_{L5_ref}	Current reference for i_{L5} [A].
i_{L6_ref}	Current reference for i_{L6} [A].
$I_{L\mathrm{max}}$	Maximum scaling current for inductance references [A].
$n_d(s)$	Low-pass filter transfer function.
τ	Time constant of low-pass filter [s].
$i_{\mathrm{fc\_droop}}$	Droop controller current command for FC [A].
i_{fc}	Measured FC current [A].
$i_{\mathrm{fc\_ref}}$	Reference FC current after droop and filtering [A].
I_{fcmax}	Maximum FC current [A].
r_{droop}	Virtual resistance in droop control [Ω].
v_{link}	Representative dc-link voltage [V].
$v_{\mathrm{link\_min}}$	Minimum representative dc-link voltage [V].
Δv_{link}	Voltage deviation for the representative dc-link [V].
$H_{\Delta v}$	Normalization gain for voltage deviation.
i_{L_fuzzy}	Generic Fuzzy-based current output [p.u.].
c	Center of Gaussian membership function.
σ	Standard deviation of Gaussian membership function.
μ	Membership function output.
μ_{SoC}	Membership function for SoC input.
μ_v	Membership function for voltage deviation input.
μ_{iL}	Membership function for current output.
$y(s)$	Output of low-pass filter in Laplace domain.
$y(t)$	Output of low-pass filter in time domain.
$\boldsymbol{x}_{\mathrm{mg}}$	State vector of the MG average model.
$\boldsymbol{u}_{\mathrm{mg}}$	Input vector of the MG average model.
$\boldsymbol{y}_{\mathrm{mg}}$	Output vector of the MG average model.
$\boldsymbol{A}_{\mathrm{mg}}$	State matrix of the MG model.
$\boldsymbol{B}_{\mathrm{mg}}$	Input matrix of the MG model.
$\boldsymbol{E}_{\mathrm{mg}}$	Output matrix of the MG model.
$\boldsymbol{D}_{\mathrm{mg}}$	Feedforward matrix of the MG model.
$H(s)$	Transfer function matrix of the system.
λ_i	Eigenvalues of the system.
$\delta\mathrm{SoC}$	Variation in SoC [%].
$\delta\mathrm{SoC}_{x\_\mathrm{cbc}}$	Variation in SoC influenced by CBC [%].
$\delta\mathrm{SoC}_{x\_\mathrm{cbb}}$	Variation in SoC influenced by CBB [%].

I. INTRODUCTION

The application of BESS units has been introduced in MGs to enhance their operation [1], [2]. This includes providing support during electrical fault, compensating fast transient, and addressing the intermittency of renewable energy sources

(RES) [3], [4]. In this context, it is essential to ensure the optimal performance of BESS operations to improve its efficiency.

As a result, strategies for balancing the SoC among BESS units are employed to prevent deep discharges, overcharges, and to coordinate operations effectively to avoid damage to the BESS units [5]. In addition, other approaches have been proposed concerning state of health and battery degradation factors to analyze the behavior and improve the BESS unit operation [6]. Moreover, some EMS methods with other RES have also been proposed to improve the reliability in MGs.

Aiming the SoC equalization methodology in an MG, most of the solutions are designed considering the SoC-based droop [7]. For instance, the SoC-based droop from [8] is associated with a high-pass filter, while Xia et al. [9] implemented droop control with the SoC modifying both the virtual resistance and the rated dc-link voltage. In addition, Wu et al. [10] employed an SoC balancing factor from the traditional droop control method, while Su et al. [11] designed an SoC-based droop to maintain dc-link voltage constant during the equalization process. Furthermore, some approaches do not take into account equalization based on droop. Nevertheless, they have the capability to operate in an MG that also receives power from other RES using droop controllers. For instance, in [12], a sigmoid function is employed to balance the SoC in the BESS units.

This approach offers the advantage of smoother and continuously differentiable functions. In a different solution, the SoC equalization is established in [13] based on the reflected Ampere-hour capacity from the BESS units. In addition, a model predictive control strategy is proposed for SoC balancing in [14] and [15], ensuring compliance with SoC constraints. However, the proposed method results in significant current oscillations, which can compromise sensitive loads and potentially damage to the membranes if an FC is included in the MG. Finally, Fagundes et al. [16] developed a solution for the BESS units using fuzzy logic to ensure the SoC equalization among them.

Taking into account the fuzzy logic for EMS, according to [17], it is not influenced by the MG nonlinearities, consequently, its complex mathematical model is not necessary. As a result, there is no need to deal with the MG topology or structure, resulting in simple rule-based linguistic structures and easy implementation [18].

As indicated by [19], fuzzy logic is suitable for BESS charging/discharging control. Considering some applications of fuzzy in MGs, Kakigano et al. [20] employed a strategy to regulate the dc voltage using a droop-based fuzzy strategy. In [21], the BESS units achieve equalization through a fuzzy inference system designed to define the virtual resistance for droop control, while Díaz et al. [22] also defined the EMS for BESS by using an SoC-based droop in which the weight factor is modified by a fuzzy inference system.

As a consequence, the drawback lies in the implementation of these strategies to evaluate the logic of the term obtained by fuzzy, which weighs the droop-based technique. In addition, there are challenges in achieving stability analysis due to fuzzy and droop control not being continuously differentiable. Moreover, according to [13] and [25], traditional droop control may influence the deviation of power sharing among converters if there is a small error in the measured current. Consequently, this can impact the equalization of the BESS units.

According to the SoC equalization review in [5], several decentralized SoC-based droop methods are designed using voltage-source configurations. However, in the approach proposed here, fuzzy logic is implemented directly to generate the current reference—i.e., it operates on a current-source basis—using the SoC of the BESS unit and the dc-link voltage as inputs, without relying on SoC-based droop control. This straightforward implementation is well-suited for MG and enhances power-sharing accuracy.

In general, most EMS strategies that include SoC balancing for BESS units are designed for architectures in which bidirectional converters are connected to a common dc-link. Nevertheless, Chen et al. [23] proposed an SoC equalization method for a shipboard MG using a modular multilevel converter. Furthermore, in [24], an SoC-based droop control is applied within a modular multilevel converter architecture, where a current-source approach is adopted to improve EMS accuracy.

Redundancy has also been employed as a strategy to reduce the impact of potential failures in power electronic converters and to mitigate risks in applications such as electric vehicles, shipboard systems, medical facilities, military operations, and aircraft [26]. As indicated by [27], a modular dc–dc converter is a redundant system that offers significant improvements in reliability. In this context, although there are many approaches that study fault-tolerant capabilities, there are not many applications regarding EMS, including the behavior of BESS units in a system that maintains power flow even after a failure or during maintenance. In addition, according to [28] and [29], the enhancement of resilience is crucial for MG applications.

The redundancy-based dc–dc converter may show similarities with a three-port dc–dc converter. However, the proposed approach operates with two BESS units as inputs, while a three-port converter is typically designed to integrate PV systems with a BESS unit [30]. Therefore, a three-port converter is not suitable for equalizing the SoC among multiple BESS units. In addition, as indicated by [31], redundant power converters can provide power during unpredictable events, but they are not designed to operate with multiple power sources or perform SoC equalization. This underscores the importance of designing a redundancy-based dc–dc converter capable of balancing the SoC among BESS units, which can be incorporated into a dc MG.

To complement the discussion of the methodologies previously presented, Table 1 provides a comparative overview of different SoC balancing approaches found in the literature. The comparison considers the adopted methodology, the presence of fault-tolerant capability, and the topology of the employed power converter. This table aims to summarize key differences, particularly highlighting how SoC equalization

TABLE 1. Comparison of SoC Balancing Methodologies Regarding Converter Topology and Fault-Tolerant Capability

References	Methodology	Fault-Tolerant Capability	Topology of Power Converter
[8]	SoC-based droop	No	Conventional
[9]	SoC-based droop	No	Conventional
[10]	SoC-based droop	No	Conventional
[11]	SoC-based droop	No	Conventional
[13]	Reflected Ampere-hour methodology	No	Conventional
[14]	Model predictive control	No	Conventional
[15]	Model predictive control	No	Conventional
[23]	Dynamic SoC-based power sharing	Yes	Modular multilevel converter
[24]	SoC-based droop	Yes	Modular multilevel converter
[12]	Non-linear function	No	Conventional
[16]	Fuzzy-based with a fixed range voltage reference	No	Conventional
This article	Fuzzy-based method without SoC-based droop	Yes	Redundancy-based

is addressed under various strategies, including conventional SoC-droop control, model predictive control, nonlinear functions, and fuzzy-based methods as well as, the proposed approach is also included for direct comparison.

Thus, this article proposes a redundancy-based dc MG composed of a CBC converter with two inputs where is connected the BESS units. In addition, a CBB converter is introduced as an auxiliary component also with two inputs sharing the same BESS units. Finally, a boost converter interfaces the FC with the main CBC dc-link. Regarding the CBC, it maintains a stable voltage on the main dc-link by providing a continuous current to the dc load. The FC operates with a droop controller, while the BESS units receive a fuzzy-based EMS for SoC balancing without SoC-based droop, as modified from [16], which has a simple implementation suitable for the redundancy-based dc MG. Moreover, the EMS at CBC is also responsible for providing power in accordance with the dc load demand, while the CBB operates with a battery-to-battery (B2B) equalization.

While fuzzy logic has been previously employed in dc MGs, most existing approaches are centered around SoC-based droop control [5]. In contrast, the proposed method operates in a fully decentralized and communication-free manner, directly generating current references from SoC and dc-link voltage deviation inputs without relying on virtual resistances. In addition, the control is designed with a redundancy-based topology, which enables both load compensation and B2B equalization using shared BESS units. This structure, combined with the ability to maintain stable operation under fault conditions and the fuzzy-based strategy, represents a contribution not previously addressed in the literature.

Regarding the stability analysis, the complete redundancy-based dc MG average model is calculated, considering the EMS and fuzzy-based method. Then, an infinity norm H_∞ and the Lyapunov's indirect method are addressed to evaluate the stability. Since these approaches require continuously differentiable functions, a Fourier series was used to fit the fuzzy-based method, while the approximation of a droop controller for the FC was achieved by applying a sigmoid function.

Therefore, the main contributions of this article are summarized as follows.

1) Incorporating redundancy into the dc MG enhances its reliability during unexpected events, such as a failure in one of the modules.
2) The fuzzy-based method is an alternative for addressing the nonlinearities related to SoC equalization and the redundancy-based dc MG.
3) The fuzzy-based method incorporates a decentralized approach, with no communication required among BESS units or among the redundant modules in the dc MG.
4) The fuzzy-based method without droop control is capable of charging or discharging the BESS units without setting the current references as positive or negative, in contrast to the methods indicated in [13] and [32].
5) Due to the fuzzy-based method being current source-based and its performance being suitable for providing a current reference, the power-sharing is accurate, and B2B equalization is possible, in contrast to [21].

The rest of this article is organized as follows. Section II presents BESS modeling and the estimation of SoC method. In Section III, the proposed redundancy-based dc MG is shown. Section IV presents the EMS with the droop controller and fuzzy-based method. In sequence, the proposed approach is proved by the stability analysis in Section V. Section VI presents the experimental results of the redundancy-based dc MG. Finally, Section VII concludes this article.

II. PRELIMINARIES

A. BESS MODELING

In this study, the BESS unit is modeled based on the first-order equivalent circuit presented in [33]. The output voltage of the BESS, denoted as v_{bat}, is expressed as

$$v_{\text{bat}} = \text{OCV} - i_{\text{bat}} r_{\text{bat}} - i_{\text{bat}} r_{\text{bat1}} \left[1 - \exp\left(-\frac{t}{r_{\text{bat1}} C_{\text{bat1}}}\right)\right] \tag{1}$$

where OCV is the open-circuit voltage, i_{bat} is the battery current, r_{bat} represents the internal resistance, and the term $r_{\text{bat1}} C_{\text{bat1}}$ captures the relaxation behavior of the BESS over time t.

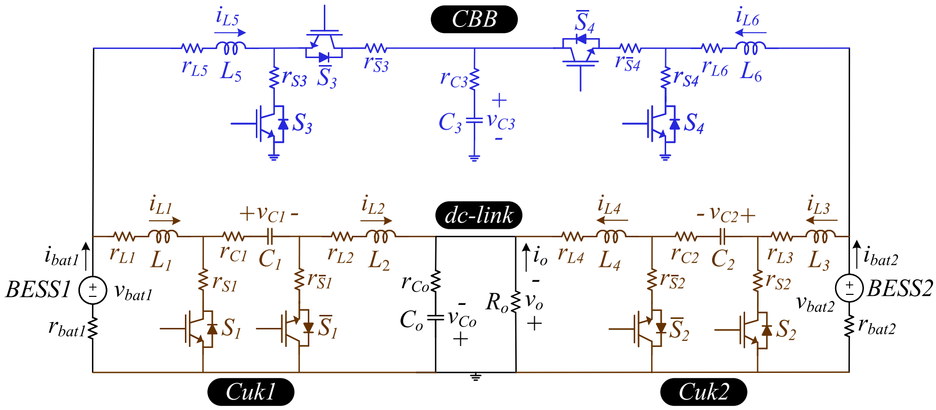

FIGURE 1. **Proposed redundancy-based DC–DC converter.**

B. ESTIMATION OF SOC

According to [34], several methods for SoC estimation exist across different approaches. Among these, the Coulomb counting method is the most commonly used, particularly in studies focusing on SoC dynamics in MGs. This method is also adopted in the present work and is expressed in the following equation:

$$\mathrm{SoC}(t) = \mathrm{SoC}(t_0) - \frac{1}{C_{\mathrm{bat}}} \int_{t_0}^{t} i_{\mathrm{bat}}(\tau_{\mathrm{bat}})\, d\tau_{\mathrm{bat}} \tag{2}$$

where $\mathrm{SoC}(t)$ represents the SoC at time t, $\mathrm{SoC}(t_0)$ is the initial SoC at the reference time t_0, C_{bat} denotes the nominal capacity of the battery, and $i_{\mathrm{bat}}(\tau_{\mathrm{bat}})$ is the battery current at time τ_{bat}.

III. REDUNDANCY-BASED DESIGNED FOR A DC MG

The proposed redundancy-based dc–dc converter is shown in Fig. 1, where the CBB module integrates 2 bidirectional boost converters using capacitance C_3, while the CBC combines Cuk1 and Cuk2 with the common output capacitance C_o.

For Cuk1, the terminal voltage and current are denoted as v_{bat1} and i_{bat1} for BESS1, while the currents i_{L1} and i_{L2} flow through inductances L_1 and L_2, and the capacitance C_1 is receiving energy from BESS1 to supply the main dc-link. In this context, the controlled semiconductor is represented by S_1 with $\bar{S}_1$ receiving the complementary PWM signals. In the case of Cuk2, the terminal voltage and current are v_{bat2} and i_{bat2} for BESS2, while inductances L_3 and L_4 carry currents i_{L3} and i_{L4}, respectively.

Similarly, the capacitance C_2 absorbs energy from BESS2 and delivers it also to the main dc-link. Considering the controlled semiconductors, represented by S_2 and $\bar{S}_2$, the former receives the PWM signals, while the latter receives the complementary PWM signals. In addition, the main dc-link includes the common capacitance C_o, the dc-link voltage identified by v_o (the voltage sensor on the dc link provides the absolute value in the HIL test-bed) and the equivalent dc load R_o is placed to obtain the output current i_o and the dc power P_{load} (expressed as $\frac{V_o^2}{R_o}$). Furthermore, the CBC (composed of Cuk converters) has the advantage of providing a continuous output current, avoiding the pulsating current that could stress sensitive loads in the main dc-link [35].

Regarding the CBB, current i_{L5} flows through L_5 and i_{L6} through L_6, active semiconductors S_3 and $\bar{S}_3$ are close to v_{bat1}, while S_4 and $\bar{S}_4$ are next to v_{bat2}, with the PWM signals of $\bar{S}_3$ and $\bar{S}_4$ being complementary to S_3 and S_4, respectively. In the CBB, its dc link includes the common capacitance C_3 and its output voltage v_{C3}.

Furthermore, Fig. 1 also includes the parasitic losses: for the inductances, they are represented by $r_{L1}, r_{L2}, r_{L3}, r_{L4}, r_{L5}, r_{L6}$; for the semiconductors, by $r_{S1}, r_{\bar{S}1}, r_{S2}, r_{\bar{S}2}, r_{S3}, r_{\bar{S}3}, r_{S4}, r_{\bar{S}4}$, and $r_{S\mathrm{fc}}$; as well as r_{C1}, r_{C2}, r_{C3}, and r_{Co} for the capacitances.

Finally, to improve the MG capability, a boost converter is connected to the main dc-link from CBC, forming the complete redundancy-based dc MG, as indicated in Fig. 2. Then, the EMS for the complete topology is addressed in Section IV.

IV. DESIGN OF THE EMS

The secondary level, known as the EMS, plays a crucial role in coordinating alternative sources within an MG by balancing the SoC of BESS units, stabilizing the dc-link voltage, controlling power exchange among sources, and assessing the operational limits of the MG [32], [36].

In this context, Fig. 2 indicates the redundancy topology responsible for the SoC equalization through the CBC and CBB units, while the FC is tied to a boost converter, which links its output to the main dc-link on CBC, ensuring a stable dc-link voltage v_o, along with CBC. Furthermore, the fuzzy-based method, designed for both CBC and CBB, can improve the operational performance of the MG, even in the presence of uncertain events or significant steps of load on the main dc-link.

A. SYSTEM CONTROL

Aiming at CBC, Fuzzy 1 receives the Δv_o (defined as the difference between the voltage on the main dc-link and the minimum voltage v_{o_min}) and the SoC_1 as inputs to compute i_{L1_fuzzy}. Then, i_{L1_fuzzy} is processed through the current gain

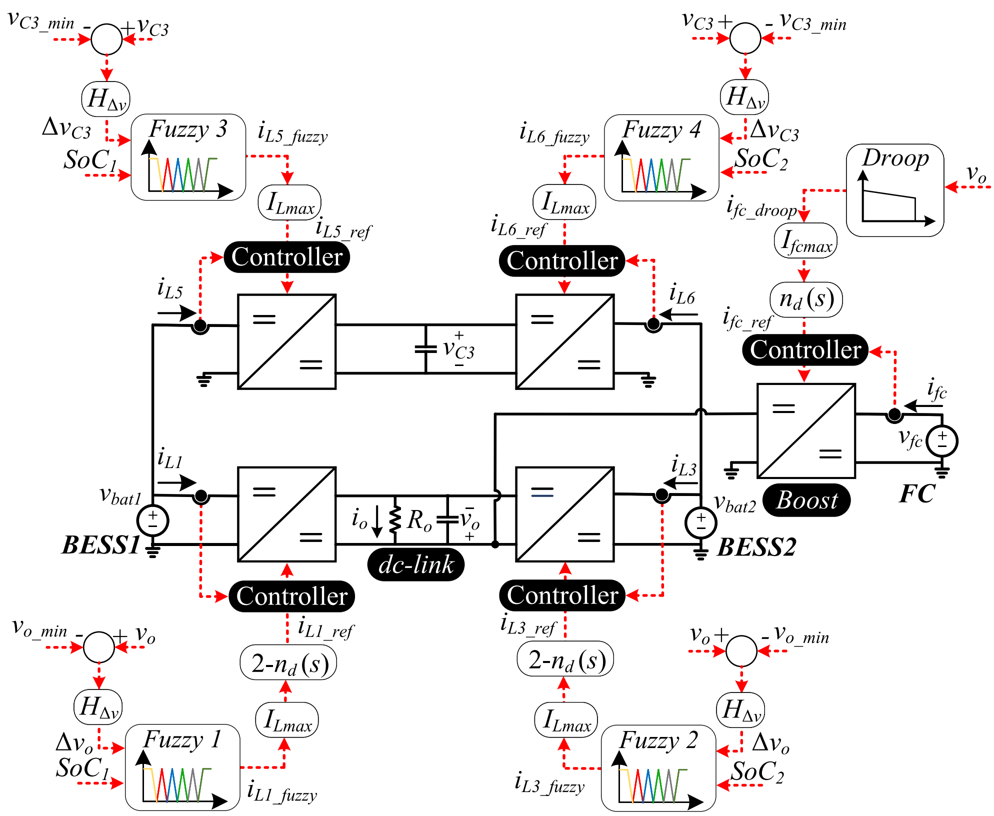

FIGURE 2. Droop and fuzzy-based method designed for the redundancy-based DC MG.

$I_{L\max}$ and a term $2 - n_d(s)$ to determine i_{L1_ref}. At steady-state regime, the low pass-filter $n_d(s)$ approaches to the unity. To prove this, consider the transfer function in (3), with τ being the time constant

$$n_d(s) = \frac{1}{1 + s\tau}. \tag{3}$$

Assume the input to the filter is a unit step function, which has a Laplace transform of $\frac{1}{s}$. The output $y(s)$ of the system is given in the following equation:

$$y(s) = n_d(s)\frac{1}{s} = \frac{1}{s(1 + s\tau)}. \tag{4}$$

To find the steady-state value of the output $y(t)$ as $t \to \infty$, it is applied the final value theorem in the following equation:

$$\lim_{t\to\infty} y(t) = \lim_{s\to 0} sy(s). \tag{5}$$

Substituting $y(s)$ from (4) into (5), it is obtained (6)

$$\lim_{t\to\infty} y(t) = \lim_{s\to 0} s\frac{1}{s(1 + s\tau)} = \lim_{s\to 0} \frac{1}{1 + s\tau} = 1. \tag{6}$$

Thus, the steady-state value of the output of the low-pass filter for a unit step input is 1. In this context, a generic current reference processed through a low-pass filter exhibits a slower dynamic response during load variation, eventually reaching steady state as the filter output approaches to the unity. In contrast, the term $1 - n_d(s)$ converges to zero, and the expression $2 - n_d(s)$ approaches 1, as expected.

Consequently, a generic current reference associated with the expression $2 - n_d(s)$ exhibits a rapid response during load variation, and then reaches steady state as the expression approaches 1. Thus, because of the expression $2 - n_d(s)$, the inductance currents that compose Cuk1 and Cuk2 (i_{L1}, a component of i_{bat1}, and i_{L3}, a component of i_{bat2}) will respond quickly to compensate load transients on the dc link, alleviating the current stress on the FC, which is associated with the low-pass filter $n_d(s)$. Therefore, the membrane of the FC is preserved from damage due to abrupt load variations.

In this context, the BESS1 can suppress the transient during load variation and continue to operate according to the fuzzy-based method. Similarly, Δv_o and the SoC_2 are the inputs for Fuzzy 2 to determine i_{L3_fuzzy}. Subsequently, i_{L3_fuzzy} is processed through the current gain $I_{L\max}$ and the term $2 - n_d(s)$ to define i_{L3_ref}. Furthermore, in the case of Fuzzy 3, it takes as inputs Δv_{C3} (which is defined as the voltage difference between v_{C3} and the minimum voltage $v_{C3\_\min}$) and SoC_1 to calculate i_{L5_fuzzy}. Subsequently, i_{L5_fuzzy} is also processed through a current gain $I_{L\max}$ to establish i_{L5_ref}. When it comes to Fuzzy 4, i_{L6_fuzzy} is generated using Δv_{C3} and SoC_2, and subsequently, it is also processed through a current gain $I_{L\max}$ to determine i_{L6_ref}. As the B2B equalization is designed for the CBB, there is no need for a high-pass filter to compensate load transients, as occurs for equalization on the CBC.

Later, the measured currents from the inductances (i_{L1}, i_{L3}, i_{L5}, and i_{L6}) are compared with each current reference (i_{L1_ref},

i_{L3_ref}, i_{L5_ref}, and i_{L6_ref}) and are subsequently handled using traditional PI controllers. As a result of the redundancy-based dc MG, the reliability of the EMS is improved, maintaining SoC equalization, even when one of the cascaded modules is under failure or maintenance.

In the case of droop controller design for the FC, the main dc-link voltage determines the current i_{fc_droop}, which then undergoes a current gain I_{fcmax} and a low-pass filter $n_d(s)$ to process i_{fc_ref}, alleviating current dynamics during dc load variations. In sequence, the PI controller processes the difference between the FC current i_{fc} and its reference i_{fc_ref}.

Finally, the redundancy-based dc MG is coordinated by the fuzzy-based method and droop controller without requiring link communication, enabling the power flow from the FC and BESS units.

B. DESIGNING OF THE DROOP CONTROL FOR THE FC

The power flow from the FC is processed by the droop controller to maintain a stable voltage on the main dc-link within the voltage range $[v_{o\_min}, v_{o\_min} + \Delta v_{o\_max}]$, with Δv_{o_max} representing the maximum voltage that Δv_o can achieve. Thus, the voltage v_o defines the current i_{fc_droop} for later processing through I_{fcmax} gain and the low-pass filter n_d (in the time-domain) to define i_{fc_ref} as indicated in the following equation:

$$i_{fc\_ref} = I_{fcmax}\left(-\frac{v_o}{\Delta v_{o\_max}} + \frac{v_{o\_min} + \Delta v_{o\_max}}{\Delta v_{o\_max}}\right) n_d. \quad (7)$$

From (7), the gain I_{fcmax} is the maximum current of the FC. In addition, the slope of the droop controller is determined by the virtual resistance defined as $r_{droop} = \Delta v_o / I_{fcmax}$.

C. REDUNDANCY-BASED FUZZY-BASED METHOD

The fuzzy-based method without droop control, initially proposed by [16], has been modified to match the voltage range defined by the designer and does not require communication between FC and BESS units. Furthermore, the adaptation of the proposed approach can also be implemented for B2B equalization within the redundant module CBB. In [16], the fuzzy logic controller is designed for a specific dc-link voltage range, whereas the proposed approach develops a fuzzy-based method suitable for any voltage range and for a B2B equalization strategy in the redundancy-based dc MG.

In this context, the fuzzy-based method incorporates the SoC and dc-link voltage as inputs, without requiring droop control for the BESS units, i.e., it is designed for the redundancy-based dc MG as indicated in Fig. 2. In addition, the proposed approach is suitable for systems with or without a dc load connected to the dc link. Consequently, the CBB can operate with B2B equalization, while the power from the CBC is determined according to the demand on the main dc-link, taking into account the SoC of the BESS units.

1) TUNING OF THE FUZZY-BASED METHOD

The fuzzy-based method is designed based on the principle that BESS units with higher SoC should supply more power than those with lower SoC, while also accounting for the necessity of regulating the dc-link voltage. Conversely, during the charging process, BESS units with lower SoC should receive a higher charging current compared to fully charged units, again considering the requirements of the dc-link voltage.

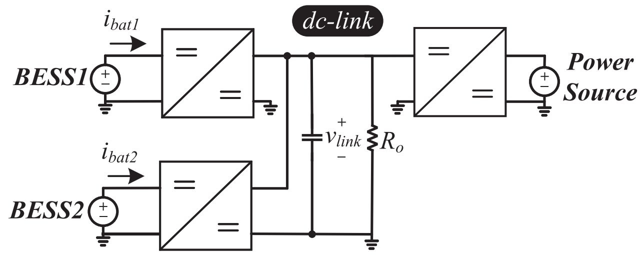

FIGURE 3. Simplified DC MG used for tuning the fuzzy-based method.

TABLE 2. BESS Action According to SoC and Δv_{link}

SoC	Δv_{link}	i_{L_fuzzy}
high (above 80%)	low demand (1 p.u.)	-0.4 to 0.0 pu
middle (around 50%)	low demand (1 p.u.)	-1.0 to -0.8 pu
low (below 30%)	low demand (1 p.u.)	-1.0 pu
high	middle demand (0.5 p.u.)	0.9 to 1.0 pu
middle	middle demand (0.5 p.u.)	0.0 pu
low	middle demand (0.5 p.u.)	-1.0 to -0.9 pu
high	high demand (0 p.u.)	1.0 pu
middle	high demand (0 p.u.)	0.9 to 1.0 pu
low	high demand (0 p.u.)	0.0 to 0.4 pu

To evaluate this concept, a simplified dc MG is considered, as illustrated in Fig. 3. This model includes an additional power source to allow testing scenarios in which both BESS units are charging. In this configuration, the dc-link voltage v_{link} and the fuzzy control current i_{L_fuzzy} (which is equal to the BESS current i_{bat}, since no additional modules are present in Fig. 3) are highlighted.

To understand the principle behind tuning the fuzzy-based method, the SoC is assumed to vary from 0% to 100%, while v_{link} operates within the range from v_{link_min} to $v_{link\_min} + \Delta v_{link}$. For normalization purposes, Δv_{link} is expressed in per unit (p.u.), ranging from 0 to 1 p.u. For instance, if the dc-link voltage operates between 200 and 220 V, then $\Delta v_{link} = 20$ V, resulting in a normalization gain of $H_{\Delta v} = 20$. In this case, a high-load condition corresponds to $\Delta v_{link} \to 0$, while a lightly loaded system leads to $\Delta v_{link} \to 1$.

The current reference i_{L_fuzzy} is also given in p.u., with -1 p.u. indicating the maximum charging current and $+1$ p.u. indicating the maximum discharging current. If the nominal BESS current is 5 A, this defines the gain I_{Lmax}. Working in the per-unit system facilitates the implementation of the fuzzy-based method across different MGs, each potentially operating with distinct current and voltage ranges.

Therefore, Table 2 summarizes the main actions of the EMS for a BESS unit, highlighting how it contributes to achieving SoC equalization, which can also guide the tuning of the fuzzy-based method. For example, BESS units that are almost

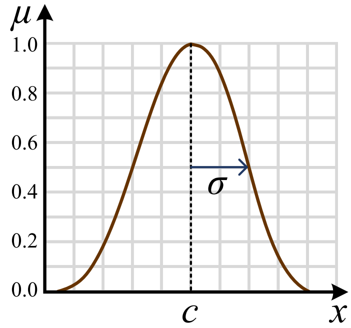

FIGURE 4. Illustration of a Gaussian function.

fully charged (above 80% SoC) will supply 1 p.u. of current when there is high demand on the dc link, whereas they will supply between −0.4 and 0.0 p.u. of current under low demand conditions. In addition, BESS units that are nearly discharged (with SoC below 30%) will provide low current (0.0 to 0.4 p.u.) during high dc-link demand and will be charged with approximately −1 p.u. when demand on the dc link is low.

Before the validation on experimental results, the fuzzy controller membership functions are conducted through simulation on MATLAB/Simulink. The goal of this assessment is to determine whether tuning is necessary for each membership function to ensure an effective equalization process. In this framework, the Gaussian function representation in (8) is utilized, guided by the information presented in Fig. 4, where σ represents the standard deviation and c denotes the mean, indicating the position of the center

$$\mu = e^{\frac{-(x-c)^2}{2\sigma^2}}. \tag{8}$$

The design of the fuzzy-based method began with the definition of equally spaced membership functions. Using the baseline actions presented in Table 2, a corresponding rule set was established. To evaluate the EMS strategy, simulations were conducted on a simplified dc MG model (see Fig. 3), where the BESS units were configured with constant SoC values. This setup allowed for isolating and analyzing the relationship between the dc-link voltage v_{link} and the current i_{L_fuzzy} (in p.u.) generated by the fuzzy-based method.

Fig. 5 outlines the complete tuning procedure. After defining the fuzzy rules, the behavior of BESS unit pairs was evaluated under different fixed SoC conditions. Next, SoC equalization was simulated using BESS units with intentionally reduced capacities to accelerate the dynamic response. Finally, small adjustments were applied to the membership functions based on the outcomes of diverse test scenarios. Although the tuning procedure may seem exhaustive, the following features help streamline the process.

1) *System symmetry:* The control behavior for charging and discharging is symmetric (i.e., the current i_{L_fuzzy} during discharging will exhibit similar behavior to charging, except for the sign). BESS units operating from 0% to 50% SoC reflect a directly opposite behavior to those from 50% to 100%. Likewise, the dc-link voltage interval Δv_{link} from 0 to 0.5 p.u. mirrors the behavior from 0.5 to 1 p.u., allowing mirrored membership functions to be defined.
2) *System closure:* The system operates within closed and bounded ranges—SoC from 0% to 100%, BESS current from −1 to 1 p.u., and Δv_{link} from 0 to 1 p.u. Operating outside these limits indicates that the load demand exceeds the capability of the dc MG. In addition, the EMS enforces saturation limits to ensure that all variables remain within these predefined boundaries. In addition, it is important to highlight that when the dc-link voltage goes outside the specified range, the control system will apply saturation based on the measured dc-link voltage. Thus, when the dc-link voltage exceeds the maximum limit, this maximum value will be used as the input to the fuzzy-based method. In contrast, when the dc-link voltage falls below the minimum limit, the minimum value will be used as the input. As a result, the fuzzy-based method can provide current reference that the inductance can support.

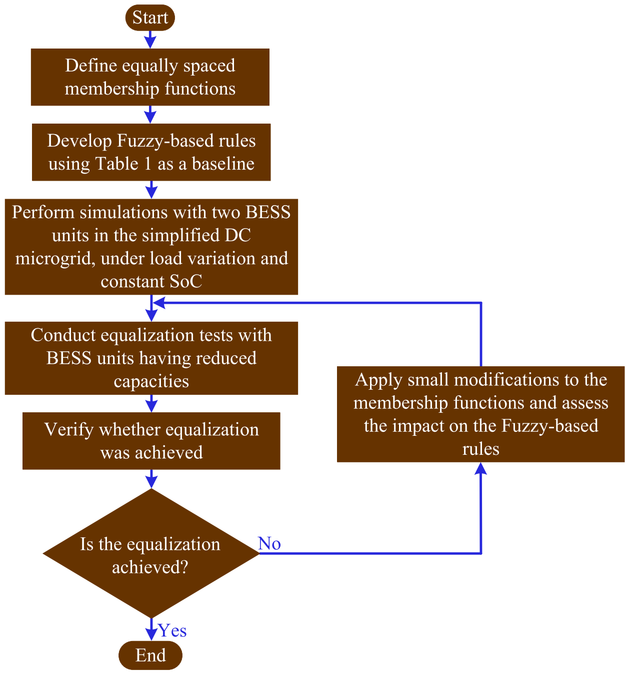

FIGURE 5. Flowchart of the fuzzy-based method procedure.

2) CURRENT REFERENCES

Thus, after the tuning process of the fuzzy-based method, the parameters σ and c for defining the membership function μ_{SoC} is outlined in Table 3 and presented in the first graph from Fig. 6. Initially, each Gaussian function is set to be equally spaced, with a mean c of 0% for "1," 25% for "2," 50% for "3," 75% for "4," and 100% for "5." Subsequently, the membership functions have their σ empirically fine-tuned.

TABLE 3. SoC Gaussian Membership

	μ_{SoC}				
	1	2	3	4	5
σ (%)	5	15	7	15	8
c (%)	0	25	50	75	100

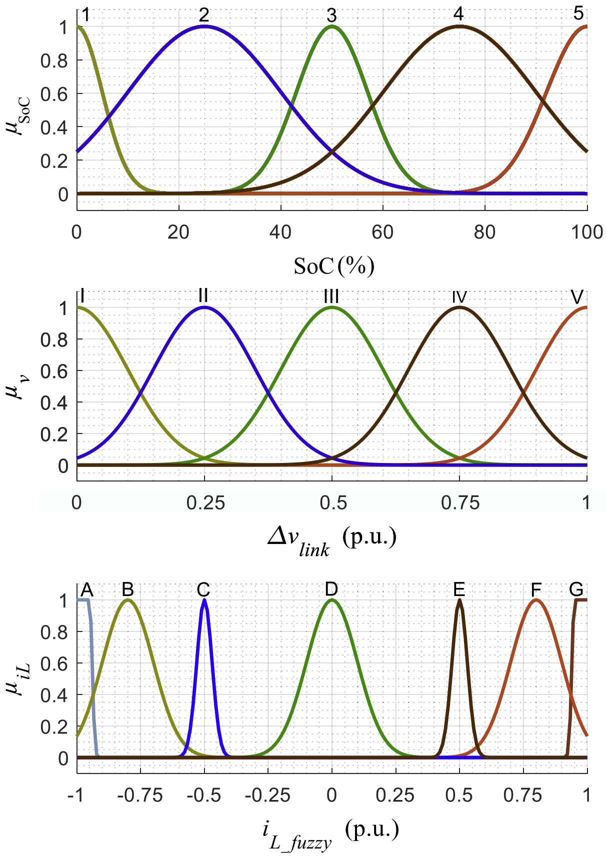

FIGURE 6. Membership functions from top to bottom: SoC (%) as input, Δv_{link} (p.u.) as input, i_{L_fuzzy} (p.u.) as output.

TABLE 4. Gaussian Membership of Δv_{link}

	μ_v				
	I	II	III	IV	V
σ (p.u.)	2	2	2	2	2
c (p.u.)	0	0.25	0.5	0.75	1

Notably, to effectively represent the BESS unit in a partially discharged and almost charged state, the linguistic variables "2" and "4" are characterized by large standard deviations (15%).

Examining the input Δv_{link}, its parameters are defined in Table 4 and illustrated in the second graph in Fig. 6. Each membership function μ_v is evenly spaced in p.u.: 0 p.u. for "I," 0.25 p.u. for "II," 0.5 p.u. for "III," 0.75 p.u. for "IV," and 1 p.u. for "V," In addition, since the load connected to the dc link has a direct proportionality to its voltage, the parameter σ is empirically set to a constant value of 2 V for optimal adjustment.

TABLE 5. Gaussian Membership of i_{L_fuzzy}

	μ_{iL}						
	A	B	C	D	E	F	G
σ (p.u.)	0.03	0.1	0.03	0.1	0.03	0.1	0.03
c (p.u.)	-1	-0.8	-0.5	0	0.5	0.8	1

TABLE 6. Rules to Design the Fuzzy-Based Method

	Δv_{link}				
SoC	**I**	**II**	**III**	**IV**	**V**
1	D	B	A	A	A
2	E	E	A	A	A
3	G	F	D	B	A
4	G	G	G	C	C
5	G	G	G	F	D

Finally, the output membership for i_{L_fuzzy} has its parameters defined in Table 5 and is shown at the bottom of Fig. 6. In this representation, the mean c is not proportionally spaced, aiming to reduce the time of SoC balance. Based on the designer's empirical adjustment, the linguistic variables "A," "C," "E," and "G" are selected with a standard deviation of 0.03 p.u, implying a slight deviation to expedite the equalization process. Meanwhile, "B," "D," and "F" are assigned a σ value of 0.1 p.u. to facilitate smooth transitions between the membership functions, where σ is set at 0.03 p.u.

Thus, the fuzzy membership functions are determined in Fig. 6, using SoC and Δv_{link} as inputs and generating the current reference i_{L_fuzzy} as an output. Initially, the measured SoC and Δv_{link} (where Δv_o is used for CBC and Δv_{C3} for CBB) are transformed into fuzzy variables by the fuzzifiers.

Subsequently, μ_{soc} and μ_v are derived from the membership functions. These values are then processed within a Mamdani's fuzzy inference system, considering the fuzzy rules in Table 6. As a result, the aggregated fuzzy set of i_{L_fuzzy} is obtained and will later be defuzzified to determine the numerical value of i_{L_fuzzy} using the center of gravity method.

Taking into account the membership functions, while the triangular shape is widely used for designing fuzzy controllers, Gaussian functions have been utilized due to their smoothness, compact notation, and suitability for engineering measurements [37], [38]. As a result, the equalization process occurs gradually, enhancing the overall reliability of the redundancy-based dc MG.

Fig. 7 presents scenarios involving pairs of BESS units operating in the simplified dc MG from Fig. 3, with slight differences in SoC—for example, $\text{SoC}_1 = 10\%$ and $\text{SoC}_2 = 0\%$—allowing for a detailed evaluation of the EMS strategy. Specifically, as follows:

1) in Fig. 7(a), the SoC values are set to $\text{SoC}_1 = 10\%$ and $\text{SoC}_2 = 0\%$;
2) in Fig. 7(b), to $\text{SoC}_1 = 90\%$ and $\text{SoC}_2 = 100\%$;
3) in Fig. 7(c), to $\text{SoC}_1 = 50\%$ and $\text{SoC}_2 = 40\%$.

In the simulation, the BESS current i_{bat} was obtained by multiplying the current reference i_{L_fuzzy} by the nominal current of the BESS units (5 A). The dc-link voltage range was set from 200 to 220 V, with $v_{\min} = 200$ V. The gain $H_{\Delta v}$

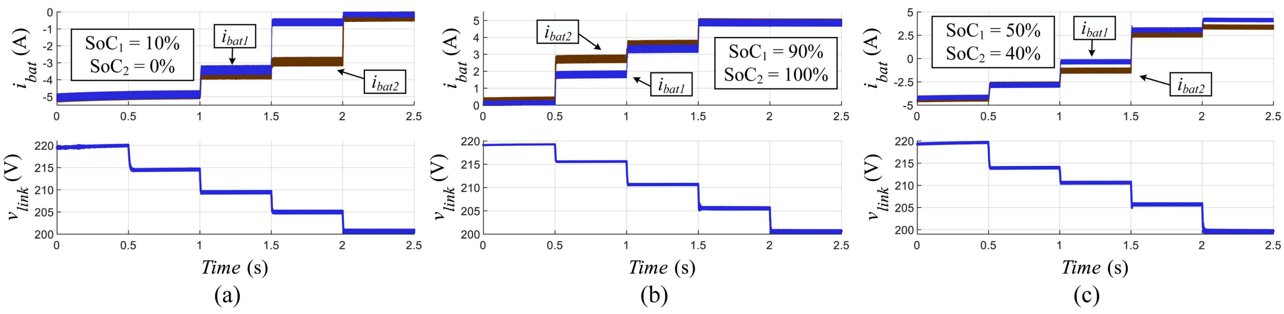

FIGURE 7. BESS current generated by the Fuzzy-based EMS for different SoC pairings between two BESS units in a simplified DC MG. Each subfigure illustrates the current sharing behavior (i_{bat1} and i_{bat2}) and DC-link voltage (v_{link}) response for a distinct SoC levels of BESS1 and BESS2: (a) SoC$_1$ = 10%, SoC$_2$ = 0%, (b) SoC$_1$ = 90%, SoC$_2$ = 100%, and (c) SoC$_1$ = 50%, SoC$_2$ = 40%.

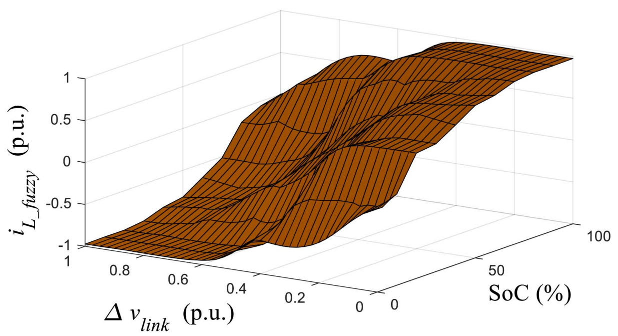

FIGURE 8. Surface generated by the fuzzy-based EMS: current reference $i_{L_{\text{fuzzy}}}$ (expressed in p.u.) as a function of SoC and DC-link voltage deviation Δv_{link} (also expressed in p.u.).

was applied to the voltage deviation Δv_{link} (expressed in p.u.) provided by the fuzzy-based method.

Thus, Fig. 7 illustrates the current behavior in response to dc load variations that produce 5 V steps at the dc link. It is observed that, at the operating boundaries, the currents from the BESS units tend to converge to similar values. Specifically, under high load demand, the BESS units supply their maximum discharge current according to their respective SoC levels (i.e., if the SoC is low, the current tends to zero). In contrast, under low load demand, the BESS units receive their maximum charging current, also depending on the SoC (i.e., if the units are already fully charged, the current tends to zero).

3) FUZZY-BASED METHOD IMPLEMENTATION

Aiming at CBC, the current i_{L1_fuzzy} is obtained from Fuzzy 1 with SoC$_1$ and Δv_o as inputs, while i_{L3_fuzzy} is calculated by Fuzzy 2 with SoC$_2$ and Δv_o as inputs. As for CBB, the currents i_{L5_fuzzy} and i_{L6_fuzzy} are obtained by using SoC$_1$ and Δv_{C3} via Fuzzy 3 and by employing SoC$_2$ and Δv_{C3} for Fuzzy 4, respectively. In addition, it is important emphasize that there are high-pass filters that process both currents on CBC to alleviate the load variation on the main dc-link, in contrast to CBB where B2B equalization is employed, as shown in Fig. 2.

Therefore, Fig. 8 depicts the 3-D surface generated by the fuzzy-based method to define the reference i_{L_fuzzy}, according to Δv_{link} and SoC. In this context, Δv_{link} is indicated within the interval [0 to 1] (represented as p.u.) and SoC is represented within the range of [0% to 100%]. Later, Fig. 9 presents different slices from the surface in Fig. 8, considering SoC as function of i_{L_fuzzy} and a constant Δv_{link}. Thus, in Fig. 9(a), the current reference represents the discharge of the BESS units when the main dc-link is under high demand ($\Delta v_{\text{link}} = 0$ p.u.), while Fig. 9(b) indicates the current reference with half demand on the dc link ($\Delta v_{\text{link}} = 0.5$ p.u.). In addition, Fig. 9(c) presents the current reference with the BESS units being charged due to the absence of load on the dc link ($\Delta v_{\text{link}} = 0$ p.u.). Thus, the fuzzy-based method encompasses the voltage variation on the dc link to define the current reference for the inductances.

Finally, the fuzzy-based method is able to equalize the BESS units in the redundancy-based dc MG, providing power in steady-state conditions while also preventing stress on the FC by allowing the BESS units to compensate for transients. First, the surface shown in Fig. 8 is discretized, and then linear interpolation is applied between the discretized points to implement the strategy in both HIL experimental results and simulation. Since the Δv_{link} was discretized in steps of 0.5 V and the SoC in steps of 0.5%, this discretization had no significant impact on EMS performance.

4) CBB FUNCTIONALITIES

The CBB is an additional module that can operate with the B2B equalization, i.e., there is no load connected to the secondary bus on C_3. Moreover, in this equalization process, Fuzzy 3 and Fuzzy 4 receive the inputs Δv_{C3} (after being processed through the voltage gain to become it expressed in p.u.) along with the SoCs of the BESS units. Subsequently, i_{L5_fuzzy} and i_{L6_fuzzy} are generated and processed through the current gain to produce the current references i_{L5_ref} and i_{L6_ref}.

Although in the ideal case (neglecting resistive losses) the relation $i_{L5} = -i_{L6}$ holds, the both inductances (L_5 and L_6) must receive the fuzzy-based method to define the equilibrium point of Δv_{C3} according to i_{L5_ref} and i_{L6_ref}, which will

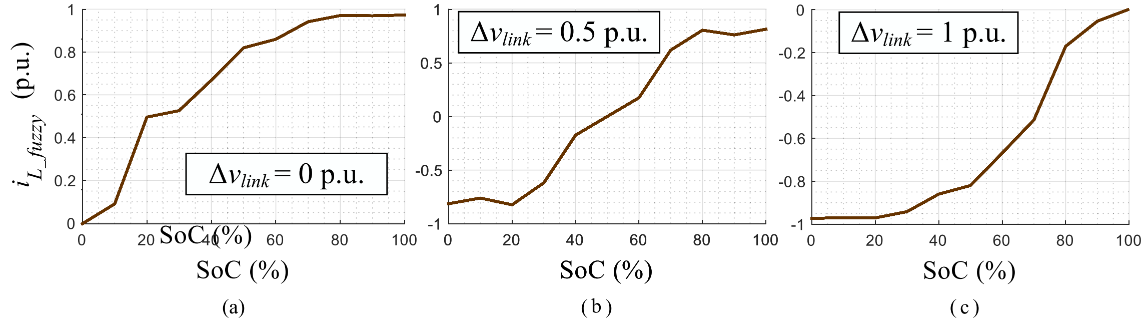

FIGURE 9. 2-D projections of the fuzzy-based EMS output $i_{L_{\text{fuzzy}}}$ as a function of SoC, for three fixed values of Δv_{link}. (a) 0 p.u. (b) 0.5 p.u. (c) 1 p.u.

determine the value of v_{C3}, as summarized in the following equation:

$$\underbrace{i_{L\_\text{fuzzy}}(\text{SoC}_1, \Delta v_{C3}) I_{L\max}}_{i_{L5\_\text{ref}}} = -\underbrace{i_{L\_\text{fuzzy}}(\text{SoC}_2, \Delta v_{C3}) I_{L\max}}_{i_{L6\_\text{ref}}}. \tag{9}$$

Furthermore, in the event of maintenance or failure in Cuk1 or Cuk2, with the EMS prioritizing the soperation on CBC and the supply of load on the main dc-link, the B2B equalization ceases, and the power flow from the damaged dc–dc converter can be redirected through the CBB. Consequently, the voltage on the main dc-link remains stable, as well as the current from the BESS units.

In conclusion, the resilience of the redundancy-based dc MG is significantly improved with the auxiliary module CBB. This is because the B2B equalization mode occurs without taking into account the dc load demanded on the main dc-link. In addition, the redundant module is also important when there is a failure in Cuk1 or Cuk2. This is crucial for redirecting the power flow from the damaged device to the CBB and ensuring the provision of power from the BESS units to the main dc-link.

5) BESS UNITS WITH DIFFERENT CAPACITIES

Since the fuzzy-based current references are defined in p.u., if BESS1 and BESS2 have different capacities, it is only necessary to multiply the p.u. current reference by a proportional scaling factor. This applies to the CBC control path. In the case of the CBB converter, which operates under a B2B strategy, a similar scaling approach is applied.

For example, consider two BESS units, one rated at 60 Ah and the other at 120 Ah.

1) *For BESS1 (60 Ah) and CBC:* $i_{L1\_\text{fuzzy}} \cdot I_{L\max}$, where i_{L1_fuzzy} is the p.u. reference and $I_{L\max}$ is the current gain.
2) *For BESS2 (120 Ah) and CBC:* $i_{L3\_\text{fuzzy}} \cdot 2I_{L\max}$, where the gain is doubled to reflect the higher capacity.
3) *For BESS1 and CBB:* $i_{L5\_\text{fuzzy}} \cdot I_{L\max}$.
4) *For BESS2 and CBB:* $i_{L6\_\text{fuzzy}} \cdot I_{L\max}$.

At first glance, it may seem that BESS2 receives a proportionally smaller B2B current compared to CBC (since i_{L6_fuzzy} is not scaled by a factor of 2). However, this interpretation can

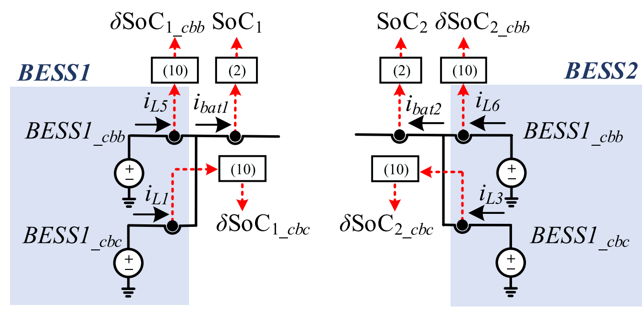

FIGURE 10. Decomposition of BESS units. Each BESS unit is virtually divided into BESS_cbc and BESS_cbb.

be clarified using the SoC estimation expression

$$\delta\text{SoC} = -\frac{1}{C_{\text{bat}}} \int_{t_0}^{t} i_L(\tau)\, d\tau \tag{10}$$

where $i_L(\tau)$ is the inductor current at time τ and considering the SoC tracking for each BESS unit

$$\text{SoC}_1 = \text{SoC}_1(t_0) + \delta\text{SoC}_{1\_\text{cbc}} + \delta\text{SoC}_{1\_\text{cbb}} \tag{11}$$

$$\text{SoC}_2 = \text{SoC}_2(t_0) + \delta\text{SoC}_{2\_\text{cbc}} + \delta\text{SoC}_{2\_\text{cbb}} \tag{12}$$

where $\delta\text{SoC}_{x\_\text{cbc}}$ and $\delta\text{SoC}_{x\_\text{cbb}}$ represent the SoC contributions from the CBC and CBB converters, respectively. Although the SoC inputs used in the EMS are SoC_1 (in Fuzzy 1 and Fuzzy 3) and SoC_2 (in Fuzzy 2 and Fuzzy 4), the individual SoC variations are determined by the inductor currents, as illustrated in Fig. 10.

1) *For SoC$_1$:* i_{L1} contributes to $\delta\text{SoC}_{1\_\text{cbc}}$, and i_{L5} contributes to $\delta\text{SoC}_{1\_\text{cbb}}$.
2) *For SoC$_2$:* i_{L3} contributes to $\delta\text{SoC}_{2\_\text{cbc}}$, and i_{L6} contributes to $\delta\text{SoC}_{2\_\text{cbb}}$.

Since the B2B equalization strategy operates with $i_{L5} \approx -i_{L6}$, it follows that $\delta\text{SoC}_{1\_\text{cbb}} \approx -\delta\text{SoC}_{2\_\text{cbb}}$. Meanwhile, the fuzzy-based method designed for the CBC must track i_{L1} and i_{L3} to complement SoC balancing for BESS1 and BESS2, even when they have different capacities.

Therefore, the system behaves as if it monitors four distinct δSoC values. The fuzzy-based method then independently

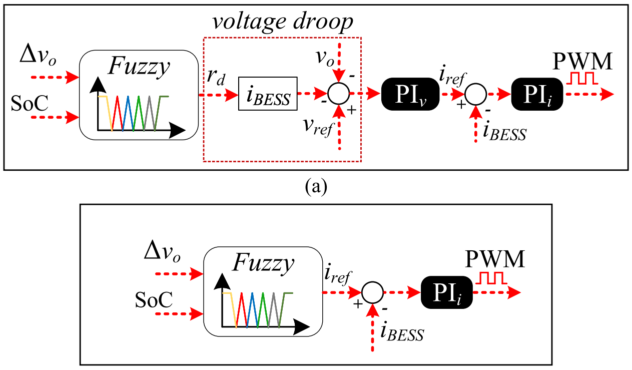

FIGURE 11. Comparison among fuzzy-based method for SoC balancing. (a) With SoC-based droop. (b) Without droop control.

generates specific current references for each virtual SoC, enabling precise equalization despite the asymmetric capacities of the BESS units.

6) COMPARISON AMONG FUZZY-BASED METHOD FOR SOC BALANCING

The proposed fuzzy-based approach operates as a current-source-based method, distinguishing it from other fuzzy-based methodologies that provide a virtual resistance as a parameter for droop control. Thus, Fig. 11(a) represents a methodology defined by [21], while Fig. 11(b) is discussed by [16] and modified for the proposed redundancy-based dc MG.

In Fig. 11, i_{ref} represents the current reference for the BESS, while i_{BESS} denotes the measured current, highlighting differences in control structure between the approaches. Taking into account the example of SoC-based droop, r_d is the virtual resistance obtained from the fuzzy-based method. Thus, in terms of implementation, while the common strategy described by [21] employs a PI controller for voltage and current control, the proposed approach is easier to implement as it does not depend on droop characteristics and allows B2B equalization without a load tied to the dc link.

V. STABILITY ANALYSIS

The stability analysis was performed using the infinity norm H_∞ and the Lyapunov's indirect method [39]. First, based on the calculations from [39] and [12], each power converter is modeled separately, considering its parameters and parasitic losses to capture its average steady-state behavior. Then, all power converters are coupled through the main dc-link voltage to form the average model of the redundancy-based dc MG. This model also incorporates the inner control loops of the converters and the EMS as the outer loop. The average model includes the fuzzy-based method, the droop controller (including voltage variation), the slow transient response of the FC, the fast response of the BESS units, and the relevant control parameters, as indicated in (13), with (14) shown at the bottom of this page, representing the interaction between the CBC and the FC boost converter in the main dc-link v_o, with parameters specified in the Appendix.

As proposed by [16], the performance of the stability analysis is achieved by approximating the fuzzy surface using the Fourier series for $i_{L\_\text{fuzzy}}(\text{SoC})$ when the dc-link is constant (v_o and v_{C3}), while it involves $i_{L\_\text{fuzzy}}(v_o)$ and $i_{L\_\text{fuzzy}}(v_{C3})$ for constant SoC. Therefore, the closed-loop performance with the infinity norm H_∞, as well as the movement of eigenvalues using Lyapunov's indirect method, is obtained from the average redundancy-based dc MG

A. EVALUATION OF CLOSED-LOOP PERFORMANCE USING THE INFINITY NORM

The infinity norm H_∞ is utilized to assess the performance of the redundancy-based dc MG, particularly evaluating the

$$\begin{bmatrix} \dot{v}_o \\ \dot{\boldsymbol{x}}_{\text{red}}^{(1:9)} \\ \dot{e}_{iL1} \\ \dot{i}_{L1\_\text{ref}} \\ \dot{e}_{iL3} \\ \dot{i}_{L3\_\text{ref}} \\ \dot{e}_{iL5} \\ \dot{e}_{iL6} \\ \dot{\boldsymbol{x}}_{\text{fc}}^{(1:2)} \\ \dot{e}_{\text{fc}} \\ \dot{i}_{\text{fc\_ref}} \end{bmatrix} = \begin{bmatrix} \text{dc}_{\text{coupled}} \\ \boldsymbol{A}_{\text{red}}(k_1,k_2,k_3,k_4)^{(1:9,1:10)}\boldsymbol{x}_{\text{red}} + \boldsymbol{B}_{\text{red}}(k_1,k_2,k_3,k_4)^{(1:9,1:2)}\boldsymbol{u}_{\text{red}} \\ 2i_{L1\_\text{fuzzy}}I_{L\max} - i_{L1\_\text{ref}} - i_{L1} \\ \frac{1}{\tau}[I_{L\max}i_{L1\_\text{fuzzy}} - i_{L1\_\text{ref}}] \\ 2i_{L3\_\text{fuzzy}}I_{L\max} - i_{L3\_\text{ref}} - i_{L3} \\ \frac{1}{\tau}[I_{L\max}i_{L3\_\text{fuzzy}} - i_{L3\_\text{ref}}] \\ i_{L5\_\text{ref}} - i_{L5} \\ i_{L6\_\text{ref}} - i_{L6} \\ \left(\boldsymbol{A}_{\text{fc10}}^{(1,1:2)} + k_{\text{fc}}\boldsymbol{A}_{\text{fck}}^{(1,1:2)}\right)\boldsymbol{x}_{\text{fc}} + \left(\boldsymbol{B}_{\text{fc0}}^{(1,1)} + k_{\text{fc}}\boldsymbol{B}_{\text{fck}}^{(1,1)}\right)\boldsymbol{u}_{\text{fc}} \\ i_{\text{fc\_ref}} - i_{\text{fc}} \\ \frac{1}{\tau}[I_{\text{fcmax}}i_{\text{fc\_droop}} - i_{\text{fc\_ref}}] \end{bmatrix} \tag{13}$$

$$\begin{aligned} \text{dc}_{\text{coupled}} = {} & \left(\boldsymbol{A}_{\text{red}}(k_1,k_2,k_3,k_4)^{(10,1:10)}\right)\boldsymbol{x}_{\text{red}} + \left(\boldsymbol{B}_{\text{red}}(k_1,k_2,k_3,k_4)^{(10,1:10)}\right)\boldsymbol{u}_{\text{red}} \\ & \cdots - \left(\boldsymbol{A}_{\text{fc0}}^{(2,1:2)} + k_{\text{fc}}\boldsymbol{A}_{\text{bfck}}^{(2,1:2)}\right)\boldsymbol{x}_{\text{fc}} - \left(\boldsymbol{B}_{\text{fc0}}^{(2,1)} + k_{\text{fc}}\boldsymbol{B}_{\text{fck}}^{(2,1)}\right)\boldsymbol{u}_{\text{fc}} - \left(-\frac{v_o}{R_oC_o}\right). \end{aligned} \tag{14}$$

dc-link voltage v_o, the inductances current i_{L1}, i_{L3}, i_{L5}, and i_{L6} and FC current i_{FC} with respect to the load current i_o. To begin, the state-space is represented in the following equation:

$$\boldsymbol{x}_{\mathrm{mg}} = \Big[v_o, \boldsymbol{x}_{\mathrm{red}}^{(1:9)}, e_{iL1}, i_{L1\_\mathrm{ref}}, e_{iL3}, i_{L3\_\mathrm{ref}}, e_{iL5}, \ldots , e_{iL6}, \boldsymbol{x}_{\mathrm{fc}}^{(1:2)}, e_{i\mathrm{fc}}, i_{\mathrm{fc\_ref}} \Big]. \quad (15)$$

Later, the state-space model matrix $\boldsymbol{A}_{\mathrm{mg}}$ is obtained from (13), as indicated in (16), with m representing the number of state-space variables

$$\boldsymbol{A}_{\mathrm{mg}} = \begin{bmatrix} \frac{\partial f1_x}{\partial x_1} & \frac{\partial f1_x}{\partial x_2} & \cdots & \frac{\partial f1_x}{\partial x_m} \\ \frac{\partial f2_x}{\partial x_1} & \frac{\partial f2_x}{\partial x_2} & \cdots & \frac{\partial f2_x}{\partial x_m} \\ \vdots & \vdots & \ddots & \vdots \\ \frac{\partial fn_x}{\partial x_1} & \frac{\partial fn_x}{\partial x_2} & \cdots & \frac{\partial fn_x}{\partial x_m} \end{bmatrix}. \quad (16)$$

Following this, $\boldsymbol{B}_{\mathrm{mg}}$ is determined by applying the Jacobian matrix to the input vector $\boldsymbol{u}_{\mathrm{mg}} = [v_{\mathrm{bat1}}, v_{\mathrm{bat2}}, v_{\mathrm{fc}}, i_o]$, as detailed in (17), with $k = 4$ (the total number of system inputs)

$$\boldsymbol{B}_{\mathrm{mg}} = \begin{bmatrix} \frac{\partial f1_x}{\partial u_1} & \frac{\partial f1_x}{\partial u_2} & \cdots & \frac{\partial f1_x}{\partial u_k} \\ \frac{\partial f2_x}{\partial u_1} & \frac{\partial f2_x}{\partial u_2} & \cdots & \frac{\partial f2_x}{\partial u_k} \\ \vdots & \vdots & \ddots & \vdots \\ \frac{\partial fn_x}{\partial u_1} & \frac{\partial fn_x}{\partial u_2} & \cdots & \frac{\partial fn_x}{\partial u_k} \end{bmatrix}. \quad (17)$$

Moreover, the output vector $\boldsymbol{y}_{\mathrm{mg}} = [i_{L1}, i_{L3}, i_{L5}, i_{L6}, \ldots, i_{\mathrm{fc}}, v_o]$ is represented in the following equation:

$$\boldsymbol{y}_{\mathrm{mg}} = \boldsymbol{E}_{\mathrm{mg}}\boldsymbol{x}_{\mathrm{mg}} + \boldsymbol{D}_{\mathrm{mg}}\boldsymbol{u}_{\mathrm{mg}}. \quad (18)$$

To achieve the desired output matrix $\boldsymbol{E}_{\mathrm{mg}}$, it is designed to be mostly zero, with elements set to 1 to identify the state-space variables that define the output vector $\boldsymbol{y}_{\mathrm{mg}}$.

The feedforward matrix $\boldsymbol{D}_{\mathrm{mg}}$ is a zero matrix of dimensions $k \times j$, where j denotes the number of outputs. A transfer function matrix, which represents the entire redundancy-based dc MG, can be derived from the state-space matrices. Therefore, the response $H(s)$ of the inductance currents i_{L1}, i_{L3}, i_{L5}, and i_{L6}, the FC current i_{FC}, and the dc-link voltage v_o (which correspond to the first through sixth inputs) with respect to the load current i_o (the sixth output) should align with the transfer function found in rows 1 through 6 and column 6.

Finally, the infinity norm is defined as $\|H(s)\|_\infty = \sup_{\omega\in\mathbb{R}} \|H(j\omega)\|$, with $H(j\omega)$ denoting the system's frequency response at frequency ω, $\|\cdot\|$ representing the magnitude, and the supremum being the maximum magnitude of the transfer function's frequency response over all possible frequencies.

1) INFINITY NORM RESPONSE FROM THE REDUNDANCY-BASED DC MG WITH B2B EQUALIZATION IN THE CBB

In this case, normal operation of the redundancy-based dc MG was considered, with B2B equalization performed through the CBB. The infinity norm from the parameters i_{L1}, i_{L3}, i_{L5}, i_{L6}, i_{fc}, and v_o over the current load i_o is defined in Table 7, with BESS units having $\mathrm{SoC}_1 = 90\%$ and $\mathrm{SoC}_2 = 10\%$. In this context, it is noted that the system maintains stability; however, robustness is not guaranteed with the infinity norm for i_{L1}, i_{L3}, i_{fc}, and v_o ($\|H(s)\|_\infty > 1$) because it depends on the P_{load} applied in the dc link.

TABLE 7. Norm Values for the Transfer Functions: Normal Operation of the Redundancy-Based DC MG

Expression	*Norm Value*
$\left\| \frac{i_{L1}(s)}{i_o(s)} \right\|_\infty$	9.3237
$\left\| \frac{i_{L3}(s)}{i_o(s)} \right\|_\infty$	3.7331
$\left\| \frac{i_{L5}(s)}{i_o(s)} \right\|_\infty$	0.0295
$\left\| \frac{i_{L6}(s)}{i_o(s)} \right\|_\infty$	0.0544
$\left\| \frac{i_{fc}(s)}{i_o(s)} \right\|_\infty$	6.9569
$\left\| \frac{v_o(s)}{i_o(s)} \right\|_\infty$	12.2311

TABLE 8. Norm Values for the Transfer Functions: Power Flow Redirection From CBC to the CBB

Expression	*Norm Value*
$\left\| \frac{i_{L1}(s)}{i_o(s)} \right\|_\infty$	1.0451
$\left\| \frac{i_{L3}(s)}{i_o(s)} \right\|_\infty$	65.5999
$\left\| \frac{i_{L5}(s)}{i_o(s)} \right\|_\infty$	25.8175
$\left\| \frac{i_{L6}(s)}{i_o(s)} \right\|_\infty$	25.9606
$\left\| \frac{i_{fc}(s)}{i_o(s)} \right\|_\infty$	4.1187
$\left\| \frac{v_o(s)}{i_o(s)} \right\|_\infty$	17.4194

2) INFINITY NORM RESPONSE FROM THE REDUNDANCY-BASED DC MG WITH POWER FLOW REDIRECTION TO THE CBB

In this scenario, the infinity norm is evaluated under a fault condition in the Cuk1 converter of the CBC, which triggers a power flow redirection to the CBB. The infinity norm values for the parameters i_{L1}, i_{L3}, i_{L5}, i_{L6}, i_{fc}, and v_o, relative to the output current i_o, are presented in Table 8, considering BESS units with $\mathrm{SoC}_1 = 90\%$ and $\mathrm{SoC}_2 = 70\%$.

Unlike the case with B2B equalization in the CBB—where robustness is maintained—the current scenario does not ensure robustness for i_{L1}, i_{L3}, i_{fc}, v_o, and the CBB parameters i_{L5} and i_{L6}, as indicated by $\|H(s)\|_\infty > 1$. This outcome depends on the applied load power P_{load} at the dc link. Moreover, due to the power flow redirection, the performance of the CBB is also affected by variations in the dc load.

Section V-B employs Lyapunov's indirect method to further investigate how P_{load} influences the maximum power capability of the redundancy-based dc MG.

B. LYAPUNOV'S INDIRECT METHOD

By applying the Jacobian matrix in (13), the movement of the eigenvalues is obtained. The analysis considers two cases: 1) $\Delta\mathrm{SoC} = \mathrm{SoC}_1 - \mathrm{SoC}_2 \rightarrow 0$, with dc load variation on the main dc-link; and 2) the size of the redundancy-based dc MG

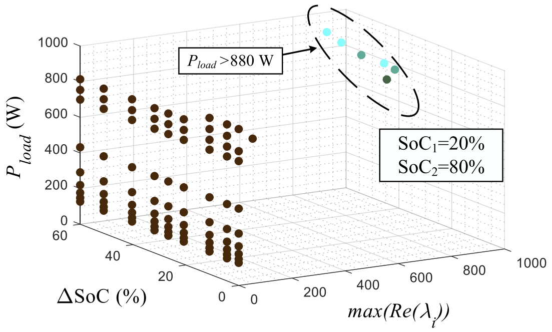

FIGURE 12. max(Re(λ_i)) as a function of the maximum power from BESS units ($P_{\mathrm{BESS1}} + P_{\mathrm{BESS2}}$) and FC ($P_{\mathrm{fc}}$).

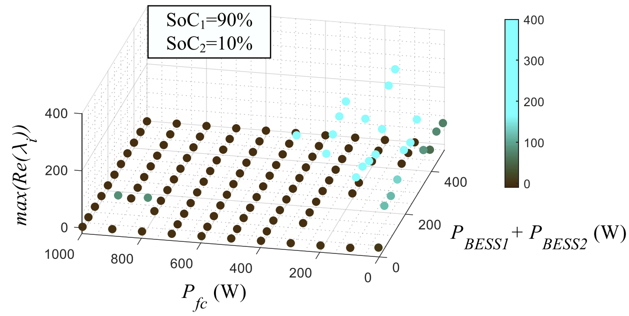

FIGURE 13. max(Re(λ_i)) as a function of load variation on the main DC-link (P_{load}) and the equalization process when ΔSoC $\to$ 0%.

by varying the maximum power from the BESS units and FC, with constant SoC and dc load.

1) EVALUATING SOC BALANCING WITH STEPS OF LOAD ON THE DC LINK

In this case, SoC balancing is analyzed with steps of load in the main dc-link. The maximum real part of the eigenvalues [max(Re(λ_i))] varies according to ΔSoC(%) (with initial values set as $\mathrm{SoC}_1 = 20\%$ and $\mathrm{SoC}_2 = 80\%$) and P_{load}, as indicated in Fig. 12. During this procedure, the initial value of P_{load} is set to 100 W, and increments of 50 W are applied until it reaches 900 W. Then, the redundancy-based dc MG is maintained stable as long as $P_{\mathrm{load}} < 880$ W, due to the max(Re(λ_i)) displaying values lower than 0 (left-side of the complex-plan).

2) SIZE OF REDUNDANCY-BASED DC MG: POWER VARIATION IN THE BESS UNITS AND FC

From this analysis, the maximum power delivered from the BESS units ($P_{\mathrm{BESS1}} + P_{\mathrm{BESS1}}$) and FC ($P_{\mathrm{fc}}$) is varied to determine their influence on the redundancy-based dc MG. Thus, the range for $P_{\mathrm{BESS1}} + P_{\mathrm{BESS1}}$ is [0 W, 500 W], while the P_{fc} is [0 W, 1,000 W], with the power on the main dc-link and the initial SoCs set as constant ($P_{\mathrm{load}} = 200$ W and $\mathrm{SoC}_1 = 90\%$ and $\mathrm{SoC}_2 = 10\%$). As a result, when the power demanded by the load and P_{BESS2} (because BESS2 should be charged) exceeds the power delivered by BESS1 and FC, the redundancy-based dc MG experiences unstable operation, because max(Re(λ_i)) is higher than zero, as indicated in Fig. 13.

3) OPERATION WITH B2B EQUALIZATION IN THE CBB

With BESS units operating at lower SoC levels ($\mathrm{SoC}_1 = 50\%$, $\mathrm{SoC}_2 = 20\%$), this scenario evaluates system behavior with the B2B active in CBB as P_{load} increases from 50 to 900 W. Fig. 14 presents the eigenvalue trajectories based on the state variables i_{L1}, i_{L2}, v_{C1}, i_{L3}, i_{L4}, and v_{C2}. Finally, it is observed that the signs of instability appear in the eigenvalues associated with i_{L1} and i_{L2} when $P_{\mathrm{load}} > 880$ W.

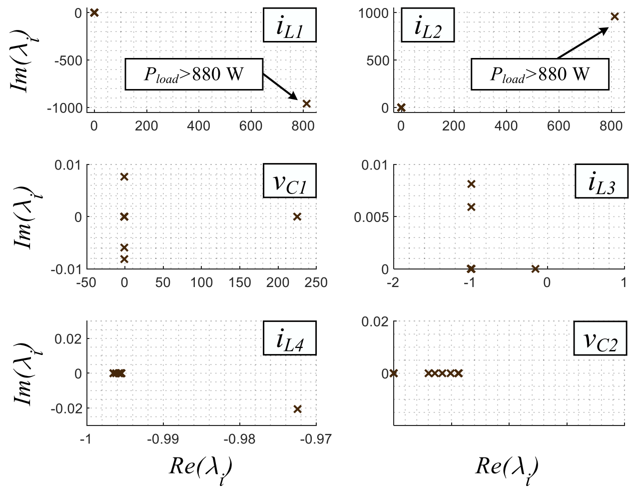

FIGURE 14. Trajectory of the most influential eigenvalues in the complex plane for constant SoC conditions ($\mathrm{SoC}_1 = 50\%$, $\mathrm{SoC}_2 = 20\%$).

4) OPERATION WITH POWER FLOW REDIRECTION TO THE CBB

Under constant SoC conditions ($\mathrm{SoC}_1 = 90\%$, $\mathrm{SoC}_2 = 70\%$), this scenario analyzes the system behavior with the B2B disabled because the power is redirected from Cuk1 to the CBB, as P_{load} varies from 50 to 900 W. Fig. 15 shows the eigenvalue trajectories derived from i_{L1}, i_{L2}, v_{C1}, i_{L3}, i_{L4}, and v_{C2}, where the instability is observed only in the eigenvalues of i_{L1} when $P_{\mathrm{load}} > 900$ W.

VI. EXPERIMENTAL RESULTS

The prototype from which the experimental results were obtained is made possible through the interaction between SpeedGoat, where the redundancy-based dc MG is constructed, and dSPACE, which is responsible for the control algorithms, as indicated in Fig. 16. Furthermore, Table 9 presents the parameters for the complete redundancy-based dc MG, including the parasitic losses of the inductances, semiconductors, and capacitances associated with the redundancy-based dc–dc converter. In addition, it includes the previously unlisted losses of the boost converter, namely the diode ($r_{D\mathrm{fc}}$), inductor ($r_{L\mathrm{fc}}$), and semiconductor switch ($r_{S\mathrm{fc}}$).

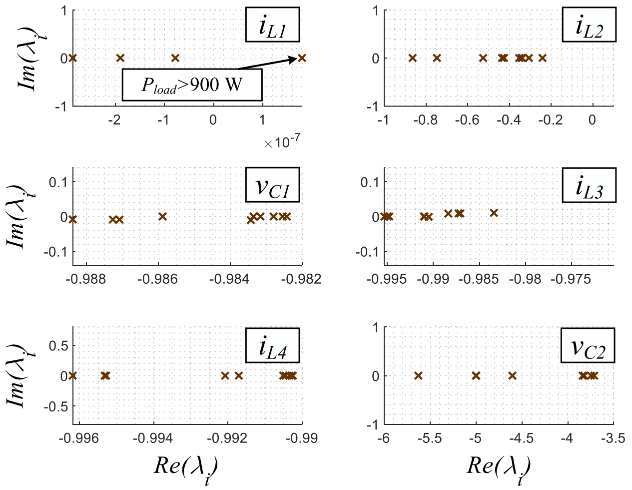

FIGURE 15. Trajectory of the most influential eigenvalues in the complex plane under constant SoC conditions ($SoC_1 = 90\%$, $SoC_2 = 70\%$), considering a failure in Cuk1 within the CBC and a power flow redirection through the CBB.

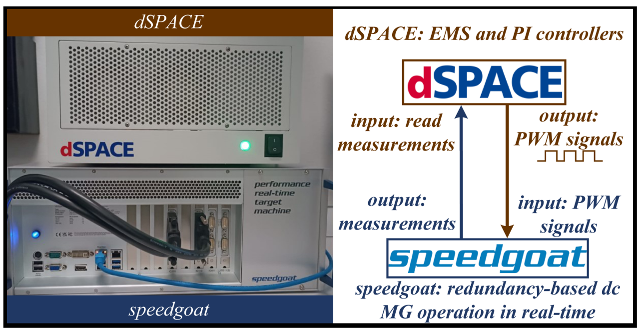

FIGURE 16. Experimental setup: interaction between SpeedGoat and dSPACE.

TABLE 9. Redundancy-Based DC MG Parameters

Component Values	
Inductances (L_1 to L_6, L_{fc})	4.8 mH
Capacitors C_1, C_2	130 μF
Capacitors C_3, C_o	470 μF
Parasitic Losses	
r_{L1} to r_{L6}, r_{Lfc}	150 mΩ
r_{S1} to r_{S4}, $r_{\bar{S}1}$ to $r_{\bar{S}4}$	30 mΩ
r_{Sfc} , r_{Dfc} , r_{C1}, r_{C2}	30 mΩ
r_{C3}, r_{CO}	150 mΩ

In addition, the switching frequency is set to 10 kHz. FC has a rated power of 1 kW and a maximum current of 20 A, based on parameters similar to the H-1000 FC from Horizon Technologies. The BESS unit is composed of a Li-Po battery pack and has a rated capacity of 60 Ah and a nominal voltage of 36 V, with a maximum charge/discharge current of 10 A. Regarding the voltage range, $-v_o$ is defined within [200 V to 220 V], v_{C3} is specified as [100 V to 120 V], with the maximum allowable variations of Δv_o and Δv_{C3} being 20 V.

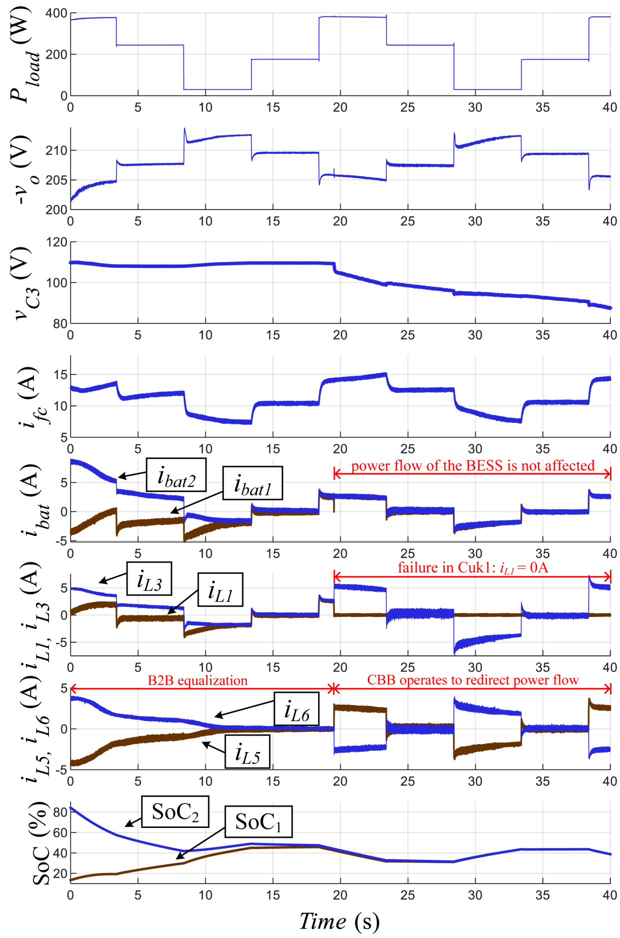

FIGURE 17. SoC equalization considering the B2B equalization, followed by a failure in Cuk1 at 19 s.

A. RELIABILITY UNDER B2B EQUALIZATION

This section assesses the performance of B2B equalization under two fault scenarios: i)a failure in a single Cuk converter (Cuk1), and ii)failures in both Cuk converters (Cuk1 and Cuk2).

1) SINGLE FAILURE IN THE REDUNDANCY-BASED DC MG

For this experimental test, the BESS units have initial values as $SoC_1 = 10\%$ and $SoC_2 = 84\%$, with their capacities decreased by a factor of 2400 to speed up the elapsed time to perform the SoC equalization. In this context, Fig. 17 indicates the steps of load $\Delta P_{\text{load}}(\approx 200$ W), the main dc-link voltage $-v_o$, v_{C3}, FC and BESS currents i_{fc}, i_{bat1}, and i_{bat2}, the inductance currents i_{L1}, i_{L3}, i_{L5}, and i_{L6} and SoCs (SoC_1 and SoC_2).

In this test, SoC equalization is achieved around 17 s after the initial operation in the experimental results. Later, a failure occurs in the redundancy-based dc MG, specifically in Cuk1 at 19 s, causing i_{L1} to drop to zero. Consequently, the power flow from the malfunctioning dc–dc converter is redirected to the CBB, stabilizing the main dc-link voltage v_o . From 0 to

19 s, the CBB operates in B2B equalization mode; however, after the failure, this mode is stopped as the CBB receives the power flow previously handled by Cuk1. As a result, v_{C3} decreases until it reaches approximately twice the voltage of the BESS unit.

During the load changes on the main dc-link, the FC undergoes smooth variations to protect and prevent damage to its membranes. Meanwhile, the BESS units are responsible for compensating and absorbing load transients, even after the failure of Cuk1. Finally, reliability is demonstrated both during the initial operation (from 0 to 19 s) in B2B equalization mode and after the failure, with the CBB designed to redirect power flow, ensuring that the dc-link voltage v_o remains stable, along with the BESS unit currents i_{bat1} and i_{bat2}.

2) DOUBLE FAILURE IN THE REDUNDANCY-BASED DC MG

In this scenario, the initial SoC values are $\text{SoC}_1 = 50\%$ for BESS1 and $\text{SoC}_2 = 90\%$ for BESS2. To accelerate the SoC equalization process, the storage capacities of both units are artificially reduced by a factor of 4800. Under these conditions, Fig. 18 presents several key parameters: the load variation $\Delta P_{\text{load}}(\approx 350$ W), the main dc-link voltage $-v_o$, the capacitor voltage v_{C3}, the currents from the FC and BESS units (i_{fc}, i_{bat1}, and i_{bat2}), the inductor currents (i_{L1}, i_{L3}, i_{L5}, and i_{L6}), and the performance of the SoC levels for both BESS units (SoC_1 and SoC_2).

In this experiment, SoC equalization begins simultaneously in CBC and CBB using B2B equalization. At 7 s, a failure occurs in Cuk2, interrupting the B2B equalization process in CBB. Consequently, power is redirected from BESS2 to CBB, flowing through inductors L_6 and L_5 and being processed by Cuk1, which results in an increase in the inductor current i_{L1}. This redirection causes slight variations in the BESS currents, though these changes are not significant, and the dc-link voltage remains stable.

At 9.2 s, a second failure takes place, now in Cuk1. As a result, with both Cuk converters in CBC out of operation, power redirection becomes unfeasible. The system then returns to B2B equalization in CBB, and the redundancy-based dc MG sustains the dc-link voltage exclusively through the FC, constrained by its maximum power capacity. At 12.5 s, CBC resumes full operation with the restoration of Cuk1 and Cuk2, allowing the redundancy-based dc MG to return to its complete configuration. The SoC equalization process is finalized around 24 s.

During this sequence, several key events are observed in Fig. 18:

i) the capacitor voltage v_{C3} drops from approximately 110 to 85 V due to the loss of B2B equalization and the initiation of power redirection in CBB;
ii) the current i_{L1} increases because it receives power from CBB while there is no current contribution from Cuk2 ($i_{L3} = 0$);
iii) both i_{L1} and i_{L3} fall to zero during the simultaneous failure of Cuk1 and Cuk2 in CBC;
iv) CBB initially performs B2B equalization;
v) CBB then transitions to power redirection, transferring energy from BESS2 to BESS1;
vi) B2B equalization resumes, with the capacitor voltage v_{C3} returning to its nominal value of approximately 110V.

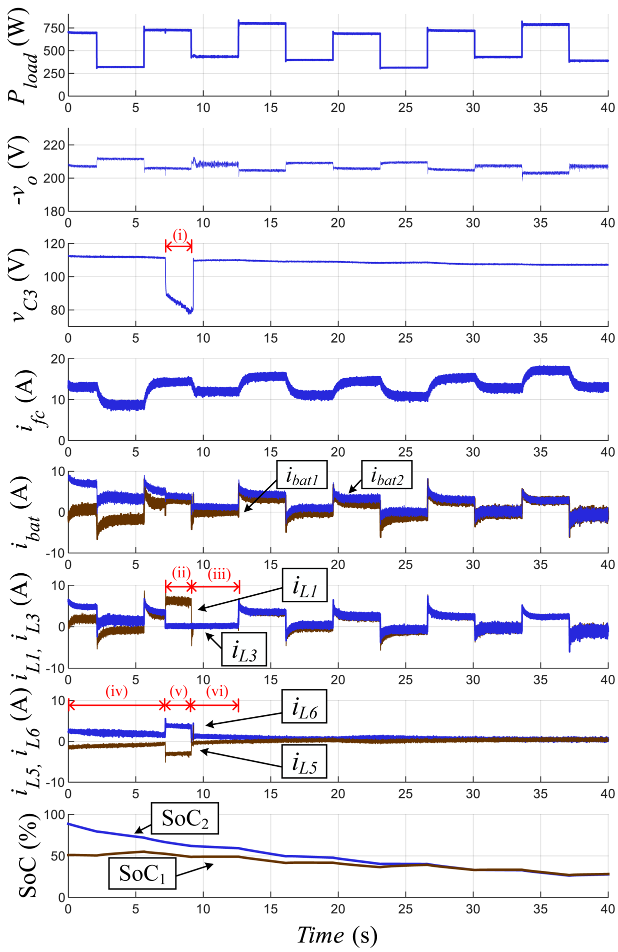

FIGURE 18. SoC equalization considering B2B equalization, followed by a failure in Cuk1 at 7.2 s and simultaneous failures in Cuk1 and Cuk2 at 9.2 s.

B. EQUALIZATION WITH BESS HAVING DIFFERENT CAPACITIES

In this experiment, BESS2 is configured with twice capacity of BESS1-that is, 120 Ah for BESS2 and 60 Ah for BESS1. In addition, the initial SoC values are set to $\text{SoC}_1 = 90\%$ for BESS1 and $\text{SoC}_2 = 10\%$ for BESS2. In this context, to speed-up the SoC equalization process, both units have their capacities scaled down by a factor of 2400. Under these conditions, Fig. 19 illustrates the system's dynamic behavior, including the load steps ΔP_{load} ($\approx$ 350 W) operating at a high switching frequency ($\approx$ 30 kHz), the main dc-link voltage $-v_o$, the capacitor voltage v_{C3}, the currents from the FC and the BESS units (i_{fc}, i_{bat1}, and i_{bat2}), the inductor currents (i_{L1}, i_{L3}, i_{L5}, and i_{L6}), and the SoC behavior leading to equalization.

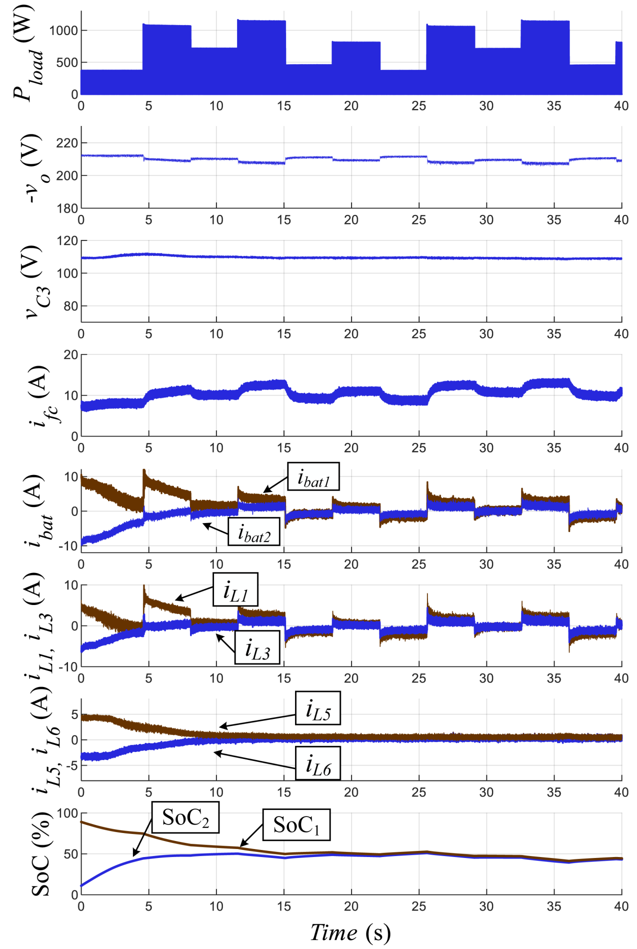

FIGURE 19. Redundancy-based dc MG operation with unequal BESS capacities (BESS1: 120 Ah; BESS2: 60 Ah) and high-frequency load steps (≈ 30 kHz) at the main dc-link with ≈ 350 W variations.

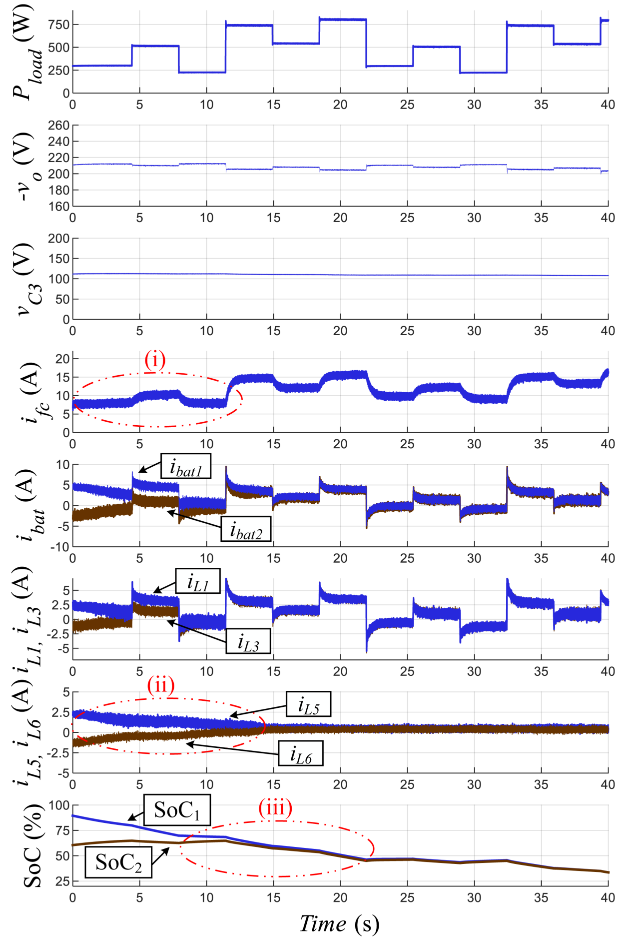

FIGURE 20. Comparison among the EMS (experimental tests): fuzzy-based method.

In this case, the scenario involving high frequency load steps does not affect the operation of the redundancy-based dc MG. This happens because the dc-link capacitor works as a low-pass filter, absorbing the high-frequency components of the load current and preventing them from propagating back to the converter output, the BESS units, or the FC.

In addition, the integration of BESS units with different capacities is supported by the EMS, as all inductor current references are provided in p.u. Specifically in the CBC, BESS1-which has twice the capacity of BESS2-must deliver a current reference for i_{L1} that is twice the magnitude of the reference for i_{L3}. This ensures a proportional energy contribution according to capacity. Furthermore, in the CBB stage, which operates using B2B equalization, it is required that i_{L5} and i_{L6} maintain equal values, since bidirectional balancing requires a symmetric current flow between the units. Regardless of these conditions, the system functions effectively with four distinct δSoC values, as detailed in Section IV-C5, allowing SoC equalization within the redundancy-based dc MG.

This behavior is evident in Fig. 19, where i_{L1} clearly exhibits higher magnitude values compared to i_{L3} during the initial interval (0 to 15 s), with i_{L3} remaining near zero while i_{L1} shows a significant deviation from the zero axis. In parallel, the B2B equalization proceeds as expected, with the waveforms of i_{L5} and i_{L6} confirming balanced current sharing. As a result, the SoC equalization is completed at approximately 17 s. Therefore, although the redundancy-based dc MG is structurally symmetrical, it is capable of achieving effective SoC balancing even when the BESS units have unequal capacities.

C. COMPARISON WITH OTHER STRATEGIES

Since most of the research in the literature evaluates SoC equalization by considering the SoC-based adaptive droop, the authors have applied the approaches proposed in [9] and [11] to compare them with the fuzzy-based method. Consequently, this SoC-based method is well-suited for B2B equalization because the rated voltage v_{C3} can be adjusted even in the absence of a load connection.

The comparison is made using initial values of $SoC_1 = 88\%$ and $SoC_2 = 60\%$, with load steps of 250 W applied to the dc link (ΔP_{load}). The fuzzy-based method is shown in Fig. 20, while the SoC-based adaptive droop approach is illustrated in Fig. 21 (from [9]) and Fig. 22 (from [11]). Considering the performance comparison with the SoC-based adaptive

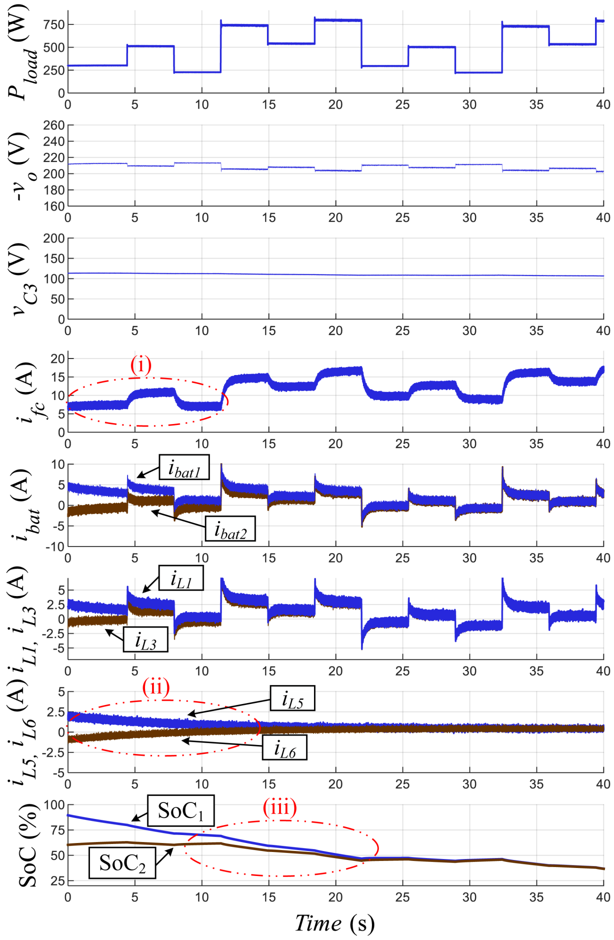

FIGURE 21. Comparison among the EMS (experimental tests): SoC-based droop from [9].

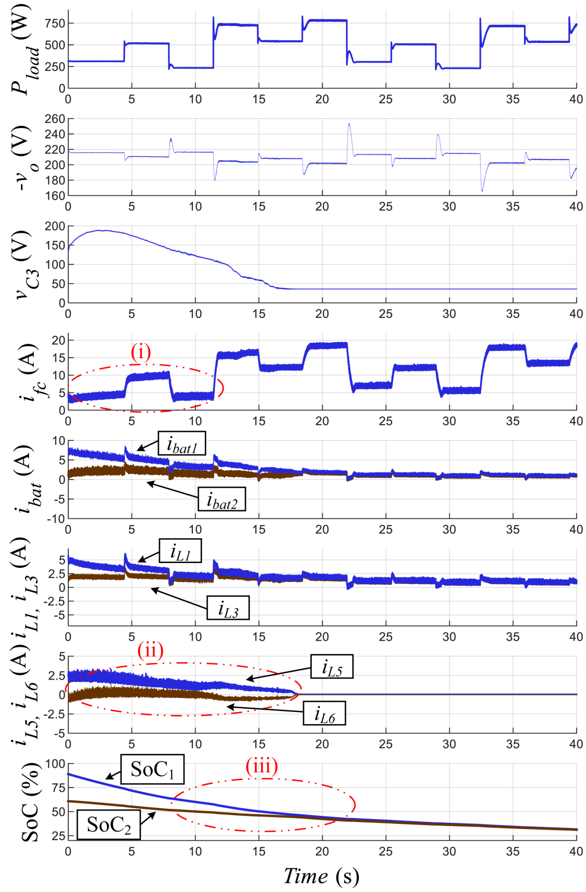

FIGURE 22. Comparison among the EMS (experimental tests): SoC-based droop from [11].

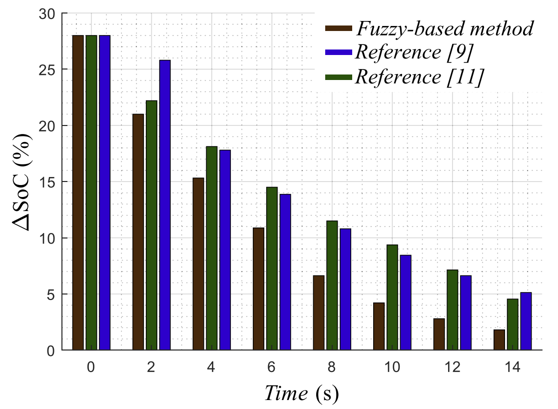

FIGURE 23. Comparison with other methodologies: the value of ΔSoC for each 2 s of step time.

droop, Fig. 23 presents the value of ΔSoC (SoC$_1$–SoC$_2$) at each 2 s time step, while Fig. 24 shows ΔSoC versus the equalization time. Overall, the proposed fuzzy-based method achieved an equalization time reduction of approximately 46% compared to [9] and 33% compared to [11].

Thus, although the strategies exhibit similar behavior, the fuzzy-based method performs more effectively, as illustrated in events (i), (ii), and (iii) in Figs. 20, 21, and 22. In event (i), i_{fc} provides more power in Fig. 20, and the B2B equalization is more effective (with higher current levels) through i_{L5} and i_{L6}, as indicated in event (ii). As a result, BESS1 and BESS2 achieve SoC equalization earlier in the proposed method, as illustrated in event (iii).

In addition, regarding the comparison with the SoC-based adaptive droop shown in Fig. 21, its behavior presents greater similarity with that of the fuzzy-based method. However, as shown in Fig. 23, the proposed fuzzy-based method reduces the ΔSoC more quickly during the equalization process. Furthermore, in comparison with Fig. 22, the main dc-link voltage ($-v_o$) exhibits significant spikes under load steps, and v_{C3} fails to remain stable during B2B equalization for this approach. Thus, the fuzzy-based method demonstrates superior performance compared to the methods evaluated from the literature.

VII. CONCLUSION

This article proposes a fuzzy-based method to balance the BESS units operating in a redundancy-based dc MG without SoC-based droop, while the FC receives a droop controller. The redundancy-based mode is formed by the connection

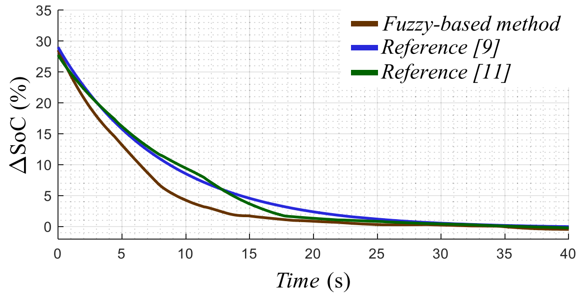

FIGURE 24. Comparison with other methodologies: ΔSoC versus time of equalization.

between CBC and CBB, sharing two BESS units in each input, while another boost converter interfaces the FC. Regarding the coordination among sources, the BESS units can provide power according to the demand on the main dc-link from CBC and also compensate for transients when there are load steps. In addition, the redundant module CBB plays a significant role in increasing reliability with B2B equalization and redirecting power flow if one of the Cuks is damaged.

First, the proposed configuration is presented, followed by the design of the fuzzy-based method and the droop controller. Subsequently, the Lyapunov's indirect method is employed to prove the stability of the proposed approach, which incorporates the fuzzy-based method approximation using a Fourier series. For the HIL implementation, the surface was discretized into points, and a linear interpolation scheme was developed for EMS execution. The EMS operation is then validated, demonstrating SoC equalization, load compensation by the BESS units, and fault tolerance during various scenarios, including a single failure in the Cuk converter, a double failure in the CBC converter, BESS units with different capacities, and the operation of the redundancy-based dc MG under high-frequency load switching. In the end, a comparison with the SoC-based adaptive droop control approaches from [9] and [11] confirms that the proposed method is significantly more efficient in operating the redundancy-based dc MG.

The generation of current references using the fuzzy-based EMS does not introduce any scalability issues, as each fuzzy controller is designed locally for its respective CBC or CBB module. This modular structure allows the approach to scale with additional BESS units without increasing the complexity of the fuzzy rule base. However, scalability challenges would arise at the system level due to increased complexity in controller coordination and the effort required for comprehensive stability analysis of the entire system.

Finally, it is important to note that this study considers ideal interconnections between BESS units and converters, without accounting for cable impedance. Thus, as future work, the integration of impedance-aware control strategies or virtual impedance compensation mechanisms will be explored to enhance the MG implementations.

APPENDIX
NOMENCLATURE FROM THE REDUNDANCY-BASED DC MG MODEL

$\boldsymbol{x}_{\text{red}}$: state vector of redundancy-based topology with $[i_{L1}\quad i_{L2}\quad v_{C1}\quad i_{L3}\quad i_{L4}\quad v_{C2}\quad i_{L5}\quad i_{L6}\quad v_{C3}\quad v_o]^T$;

$\dot{\boldsymbol{e}}_{iL1}$, $\dot{\boldsymbol{e}}_{iL3}$, $\dot{\boldsymbol{e}}_{iL5}$, $\dot{\boldsymbol{e}}_{iL6}$, and $\dot{\boldsymbol{e}}_{\text{fc}}$: current error $\dot{e}_{iL} = i_{L\_\text{ref}} - i_L$ and $\dot{e}_{\text{fc}} = i_{\text{fc\_ref}} - i_{\text{fc}}$.

$\boldsymbol{u}_{\text{red}}$ and $\boldsymbol{u}_{\text{fc}}$: input vectors of the redundancy-based topology and boost converter of FC defined as $[v_{\text{bat1}}\quad v_{\text{bat2}}\quad v_o]^T$ and $[v_{\text{fc}}{}^T]$.

$\boldsymbol{x}_{\text{fc}}$: state vector from FC defined as $[i_{fc}\quad v_o]^T$.

$\boldsymbol{A}_{red}(k_1, k_2, k_3, k_4)$: state space from the redundancy-based topology as a function of the PWM duty cycles k_1, k_2, k_3, and k_4. The matrix indices (1:9,1:10) neglect the parameters related to $\dot{v}_o$, while (10,1:10) consider them.

$\boldsymbol{B}_{red}(k_1, k_2, k_3, k_4)$: Input matrix with indices (1,1) includes terms related to the main dc-link voltage, while (2, 1) excludes them.

$\boldsymbol{A}_{fc} = \boldsymbol{A}_{fc0} + k_{fc}\boldsymbol{A}_{fck}$: State-space model of FC. The matrix indices (1,1:2) take into account the terms related to $\dot{v}_o$, while (2,1:2) exclude them.

$\boldsymbol{B}_{fc} = \boldsymbol{B}_{fc0} + k_{fc}\boldsymbol{B}_{fck}$: Input matrix of the FC with indices (2, 1) excludes parameters related to $\dot{v}_o$, while (1, 1) includes them.

$(-\frac{v_o}{R_o C_o})$: DC-link coupling between boost converter (FC) and CBC.

REFERENCES

[1] S.-Y. Chen and C.-H. Chang, "Optimal power flows control for home energy management with renewable energy and energy storage systems," *IEEE Trans. Energy Convers.*, vol. 38, no. 1, pp. 218–229, Mar. 2023, doi: 10.1109/TEC.2022.3198883.

[2] P. Lin, T. Zhao, B. Wang, Y. Wang, and P. Wang, "A semi-consensus strategy toward multi-functional hybrid energy storage system in DC microgrids," *IEEE Trans. Energy Convers.*, vol. 35, no. 1, pp. 336–346, Mar. 2020, doi: 10.1109/TEC.2019.2936120.

[3] A. C R and U. B. Manthati, "A hybrid controller assisted voltage regulation and power splitting strategy for battery/supercapacitor system in isolated DC microgrid," *IEEE Trans. Energy Convers.*, vol. 38, no. 3, pp. 1544–1553, Sep. 2023, doi: 10.1109/TEC.2023.3270292.

[4] B. Huang, S. Zheng, R. Wang, H. Wang, J. Xiao, and P. Wang, "Distributed optimal control of DC microgrid considering balance of charge state," *IEEE Trans. Energy Convers.*, vol. 37, no. 3, pp. 2162–2174, Sep. 2022, doi: 10.1109/TEC.2022.3169462.

[5] T. A. Fagundes et al., "Battery energy storage systems in microgrids: A review of SoC balancing and perspectives," *IEEE Open J. Ind. Electron. Soc.*, vol. 5, pp. 961–992, 2024, doi: 10.1109/OJIES.2024.3455239.

[6] N. Li, F. Gao, T. Hao, Z. Ma, and C. Zhang, "SOH balancing control method for the MMC battery energy storage system," *IEEE Trans. Ind. Electron.*, vol. 65, no. 8, pp. 6581–6591, Aug. 2018, doi: 10.1109/TIE.2017.2733462.

[7] M. Al-Saadi, M. Al-Greer, and M. Short, "Strategies for controlling microgrid networks with energy storage systems: A review," *Energies*, vol. 14, no. 21, 2021, Art. no. 7234, doi: 10.3390/en14217234.

[8] X. Lin, R. Zamora, and C. A. Baguley, "A fully filter-based decentralized control with state of charge balancing strategy for battery energy storage systems in autonomous DC microgrid applications," *IEEE Access*, vol. 9, pp. 15028–15040, 2021, doi: 10.1109/ACCESS.2021.3052924.

[9] Y. Xia, M. Yu, P. Yang, Y. Peng, and W. Wei, "Generation-storage coordination for islanded DC microgrids dominated by PV generators," *IEEE Trans. Energy Convers.*, vol. 34, no. 1, pp. 130–138, Mar. 2019, doi: 10.1109/TEC.2018.2860247.

[10] Q. Wu, R. Guan, X. Sun, Y. Wang, and X. Li, "SoC balancing strategy for multiple energy storage units with different capacities in islanded microgrids based on droop control," *IEEE Trans. Emerg. Sel. Topics Power Electron.*, vol. 6, no. 4, pp. 1932–1941, Dec. 2018, doi: 10.1109/JESTPE.2018.2789481.

[11] J. Su, K. Li, Y. Li, C. Xing, and J. Yu, "A novel state-of-charge-based droop control for battery energy storage systems to support coordinated operation of DC microgrids," *IEEE Trans. Emerg. Sel. Topics Power Electron.*, vol. 11, no. 1, pp. 312–324, Feb. 2023, doi: 10.1109/JESTPE.2022.3149398.

[12] T. A. Fagundes, G. H. F. Fuzato, C. R. De Aguiar, K. D. A. Ottoboni, M. Biczkowski, and R. Q. Machado, "Management and equalization of energy storage devices for DC microgrids using a SoC-sharing function," *IEEE Access*, vol. 8, pp. 78576–78589, 2020, doi: 10.1109/ACCESS.2020.2990191.

[13] R. Bhosale, R. Gupta, and V. Agarwal, "A novel control strategy to achieve SoC balancing for batteries in a DC microgrid without droop control," *IEEE Trans. Ind. Appl.*, vol. 57, no. 4, pp. 4196–4206, Jul./Aug. 2021, doi: 10.1109/TIA.2021.3073376.

[14] G. A. H. Pawitan and J.-S. Kim, "MPC-based power management of renewable generation using multi-ESS guaranteeing SoC constraints and balancing," *IEEE Access*, vol. 8, pp. 12897–12906, 2020, doi: 10.1109/ACCESS.2019.2962807.

[15] T. Morstyn, B. Hredzak, R. P. Aguilera, and V. G. Agelidis, "Model predictive control for distributed microgrid battery energy storage systems," *IEEE Trans. Control Syst. Technol.*, vol. 26, no. 3, pp. 1107–1114, May 2018, doi: 10.1109/TCST.2017.2699159.

[16] T. A. Fagundes, G. H. F. Fuzato, P. G. B. Ferreira, M. Biczkowski, and R. Q. Machado, "Fuzzy controller for energy management and SoC equalization in DC microgrids powered by fuel cell and energy storage units," *IEEE J. Emerg. Sel. Topics Ind. Electron.*, vol. 3, no. 1, pp. 90–100, Jan. 2022, doi: 10.1109/JESTIE.2021.3088419.

[17] H. Ying, "Basic fuzzy mathematics for fuzzy control and modeling," in *Fuzzy Control and Modeling: Analytical Foundations and Applications*. Hoboken, NJ, USA: Wiley, 2000, pp. 1–14.

[18] D. Arcos-Aviles et al., "An energy management system design using fuzzy logic control: Smoothing the grid power profile of a residential electro-thermal microgrid," *IEEE Access*, vol. 9, pp. 25172–25188, 2021, doi: 10.1109/ACCESS.2021.3056454.

[19] M. Faisal, M. A. Hannan, P. J. Ker, and M. N. Uddin, "Backtracking search algorithm based fuzzy charging-discharging controller for battery storage system in microgrid applications," *IEEE Access*, vol. 7, pp. 159357–159368, 2019, doi: 10.1109/ACCESS.2019.2951132.

[20] H. Kakigano, Y. Miura, and T. Ise, "Distribution voltage control for DC microgrids using fuzzy control and gain-scheduling technique," *IEEE Trans. Power Electron.*, vol. 28, no. 5, pp. 2246–2258, May 2013, doi: 10.1109/TPEL.2012.2217353.

[21] N. L. Diaz, T. Dragičević, J. C. Vasquez, and J. M. Guerrero, "Intelligent distributed generation and storage units for DC microgrids—a new concept on cooperative control without communications beyond droop control," *IEEE Trans. Smart Grid*, vol. 5, no. 5, pp. 2476–2485, Sep. 2014, doi: 10.1109/TSG.2014.2341740.

[22] N. L. Díaz, J. C. Vasquez, and J. M. Guerrero, "A communication-less distributed control architecture for islanded microgrids with renewable generation and storage," *IEEE Trans. Power Electron.*, vol. 33, no. 3, pp. 1922–1939, Mar. 2018, doi: 10.1109/TPEL.2017.2698023.

[23] P. Chen, F. Xiao, J. Liu, Z. Zhu, and Q. Ren, "Unbalanced operation principle and fast balancing charging strategy of a cascaded modular multilevel converter–bidirectional DC–DC converter in the shipboard applications," *IEEE Trans. Transport. Electrific.*, vol. 6, no. 3, pp. 1265–1278, Sep. 2020, doi: 10.1109/TTE.2020.3016029.

[24] K. Bi, S. Zhang, Y. Zhu, W. Huang, W. Lu, and Q. Fan, "An improved SOC balancing strategy for HVDC modular energy storage system based on low bandwidth communication with enhanced current regulation accuracy," *IEEE Trans. Energy Convers.*, vol. 36, no. 4, pp. 3355–3364, Dec. 2021, doi: 10.1109/TEC.2021.3082300.

[25] P. Prabhakaran, Y. Goyal, and V. Agarwal, "Novel nonlinear droop control techniques to overcome the load sharing and voltage regulation issues in DC microgrid," *IEEE Trans. Power Electron.*, vol. 33, no. 5, pp. 4477–4487, May 2018, doi: 10.1109/TPEL.2017.2723045.

[26] A. Bakeer, A. Chub, and D. Vinnikov, "Self-healing photovoltaic microconverter with zero redundancy and accurate low-cost fault detection," *IEEE Trans. Ind. Electron.*, vol. 71, no. 1, pp. 646–656, Jan. 2024, doi: 10.1109/TIE.2023.3250836.

[27] W. Zhang, D. Xu, P. N. Enjeti, H. Li, J. T. Hawke, and H. S. Krishnamoorthy, "Survey on fault-tolerant techniques for power electronic converters," *IEEE Trans. Power Electron.*, vol. 29, no. 12, pp. 6319–6331, Dec. 2014, doi: 10.1109/TPEL.2014.2304561.

[28] M. Faisal, M. A. Hannan, P. J. Ker, M. S. Hossain Lipu, and M. N. Uddin, "Fuzzy-based charging–discharging controller for lithium-ion battery in microgrid applications," *IEEE Trans. Ind. Appl.*, vol. 57, no. 4, pp. 4187–4195, Jul./Aug. 2021, doi: 10.1109/TIA.2021.3072875.

[29] M. A. Hannan, M. G. M. Abdolrasol, M. Faisal, P. J. Ker, R. A. Begum, and A. Hussain, "Binary particle swarm optimization for scheduling MG integrated virtual power plant toward energy saving," *IEEE Access*, vol. 7, pp. 107937–107951, 2019, doi: 10.1109/ACCESS.2019.2933010.

[30] Z. Wang, Q. Luo, Y. Wei, D. Mou, X. Lu, and P. Sun, "Topology analysis and review of three-port DC–DC converters," *IEEE Trans. Power Electron.*, vol. 35, no. 11, pp. 11783–11800, Nov. 2020, doi: 10.1109/TPEL.2020.2985287.

[31] M. Gleissner and M. M. Bakran, "Design and control of fault-tolerant nonisolated multiphase multilevel DC–DC converters for automotive power systems," *IEEE Trans. Ind. Appl.*, vol. 52, no. 2, pp. 1785–1795, Mar./Apr. 2016, doi: 10.1109/TIA.2015.2497218.

[32] T. R. Oliveira, W. W. A. Gonçalves Silva, and P. F. Donoso-Garcia, "Distributed secondary level control for energy storage management in DC microgrids," *IEEE Trans. Smart Grid*, vol. 8, no. 6, pp. 2597–2607, Nov. 2017, doi: 10.1109/TSG.2016.2531503.

[33] J. Su and K. Li, "Differential power processing based control framework for multiple battery energy storage systems in DC microgrids," *IEEE Trans. Sustain. Energy*, vol. 15, no. 4, pp. 2417–2427, Oct. 2024, doi: 10.1109/TSTE.2024.3421358.

[34] R. Xiong, J. Cao, Q. Yu, H. He, and F. Sun, "Critical review on the battery state of charge estimation methods for electric vehicles," *IEEE Access*, vol. 6, pp. 1832–1843, 2018, doi: 10.1109/ACCESS.2017.2780258.

[35] H.-T. Yang, H.-W. Chiang, and C.-Y. Chen, "Implementation of bridgeless CuK power factor corrector with positive output voltage," *IEEE Trans. Ind. Appl.*, vol. 51, no. 4, pp. 3325–3333, Jul./Aug. 2015, doi: 10.1109/TIA.2015.2409253.

[36] D. I. Brandao, R. P. d. Santos, W. W. A. G. Silva, T. R. Oliveira, and P. F. Donoso-Garcia, "Model-free energy management system for hybrid alternating current/direct current microgrids," *IEEE Trans. Ind. Electron.*, vol. 68, no. 5, pp. 3982–3991, May 2021, doi: 10.1109/TIE.2020.2984993.

[37] A. Sadollah, "Introductory chapter: Which membership function is appropriate in fuzzy system?," in *Fuzzy Logic Based in Optimization Methods and Control Systems and Its Applications*, A. Sadollah, Ed. Rijeka, Croatia: IntechOpen, 2018, ch. 1, pp. 1–6.

[38] V. Olunloyo, A. Ajofoyinbo, and O. Ibidapo-Obe, "On development of fuzzy controller: The case of Gaussian and triangular membership functions," *J. Signal Inf. Process.*, vol. 2, pp. 257–265, Jan. 2011, doi: 10.4236/jsip.2011.24036cite26.

[39] G. H. F. Fuzato et al., "Droop K-sharing function for energy management of DC microgrids," *IEEE J. Emerg. Sel. Topics Ind. Electron.*, vol. 2, no. 3, pp. 257–266, Jul. 2021, doi: 10.1109/JESTIE.2021.3074889.

THALES AUGUSTO FAGUNDES was born in Jundiaí, Brazil. He received the B.S. degree in electrical engineering in 2017 and the M.S. and Ph.D. degrees in electrical engineering with a focus on Dynamic Systems in 2020 and 2025, respectively, from the University of São Paulo, São Carlos, Brazil.

In 2014, he studied abroad at the University of New South Wales, Sydney, NSW, Australia, focusing on courses related to alternative energy sources. From 2022 to 2023, he was a visiting Researcher with Aalborg University, Aalborg, Denmark. He is currently a Postdoctoral Researcher with the University of São Paulo. His main research interests are in the fields of microgrids, energy management, and dc–dc converters for renewable energy sources and storage systems.

LUCAS JONYS RIBEIRO SILVA (Student Member, IEEE) was born in Viçosa, Brazil, in 1997. He received the B.S. degree in electrical engineering in 2020 from the Federal University of Viçosa, Viçosa, Brazil, and the M.S. degree in power electronics and control systems in 2022 from the University of São Paulo, São Carlos, Brazil, where he is currently working toward the Ph.D. degree in electrical engineering.

His main research interest are in the fields of microgrids, electric and hybrid vehicles, energy management and dc–dc converters for renewable energy sources and storage systems.

MÁRCIO VON RONDOW CAMPOS was born in Caratinga, Brazil. He received the B.S. degree in electrical engineering in 2022 from the Federal University of Viçosa, Viçosa, Brazil, and the M.S. degree in power electronics in 2024 from the University of São Paulo, São Carlos, Brazil, where he is currently working toward the Ph.D. degree in electrical engineering.

His mains research interest are in the fields of dc–dc converters for renewable energy sources, microgrids, energy management, and hybrid electric vehicles.

MARINA SILVA CAMILLO DE CARVALHO received the bachelor's degree in electrical engineering from the Federal University of Mato Grosso, Cuiabá, Brazil, in 2015, the master's degree in electrical engineering from the School of Engineering of São Carlos, University of São Paulo, São Carlos, Brazil, in 2017, and the Ph.D. degree in electrical engineering with a specialization in dynamic systems from University of São Paulo in 2024.

She is currently a BESS Engineer with Grupo Moura, Belo Jardim, Brazil, focusing on the development and implementation of large-scale battery energy storage systems. Her primary areas of expertise include microgrid control and management, power system optimization, and the integration of renewable energy sources.

BRUNO MENEGHEL ZILLI was born in Medianeira, Brazil. He received the B.S. degree in electronic engineering from the Federal University of Technology-Paran, Guarapuava, Brazil, in 2015, the M.S. degree in energy in agriculture engineering from Western Paraná State University, Cascavel, Brazil, in 2018, and the Ph.D. degree in electrical engineering from the University of São Paulo, São Carlos, Brazil, in 2024.

He is currently a Professor with the Federal University of Technology—Paraná. His main research interest are in the fields of microgrids, harmonic compensation, energy management, and dc–ac converters for renewable energy sources.

GUILHERME HENRIQUE FAVARO FUZATO (Member, IEEE) received the B.S. degree in electrical engineering and the M.S. and Ph.D. degrees in electrical engineering from the University of São Paulo, São Carlos, Brazil, in 2011, 2015, and 2019, respectively.

From 2018 to 2019, he was a Visiting Researcher with Aalborg University, Aalborg, Denmark. He was a Field Service Engineer with Siemens from 2012 to 2013, and as an R&D Engineer with Robert Bosch Ltda/IEL/CNPq under the InovaTalentos Fellowship from 2014 to 2015. From 2016 to 2025, he was an Assistant Professor with the Federal Institute of Education, Science and Technology, São Paulo, Brazil. He is currently an Assistant Professor with the School of Electrical and Computer Engineering, University of Campinas (UNICAMP), Campinas, Brazil. His research interests include microgrids, energy management, and dc–dc converters for renewable energy and energy storage systems.

RICARDO QUADROS MACHADO (Senior Member, IEEE) was born in Santa Maria, Brazil. He received the B.S. degree in electrical engineering from the University of Santa Maria, Santa Maria, Brazil, in 1997, and the M.S. and Ph.D. degrees in power electronics from the University of Campinas, Campinas, Brazil, 2000 and 2005, respectively.

From 2002 to 2003, he was a Visiting Researcher with the University of Padova, Padova, Italy, and from 2005 to 2007, he was a Postdoctorate with the Federal University of Santa Maria, Santa Maria, Brazil. From 2013 to 2014, he was a Visiting Professor with the University of Toronto, Toronto, ON, Canada. From 2007 to 2018, he was also an Assistant Professor with the University of Sao Paulo, Sao Carlos, Brazil. He is currently an Associate Professor with the University of Sao Paulo and his main research interests are: processing of energy in dc–dc and dc–ac converters, digital control of power converters, distributed generation systems, smart grids, and control of renewable energy sources.

Open Access provided by 'Coordenação de Aperfeiçoamento de Pessoal de Nível Superior (CAPES) - ROR identifier: 00x0ma614' within the CRUI CARE Agreement